Incorporation of Benzobisoxazole Cruciforms into Metal-Organic Frameworks and the Development of Fluoride Sensors Based on Benzobisoxazole Cruciforms

---

A Thesis Presented to

the Faculty of the Department of Chemistry

University of Houston

In Partial Fulfillment

of the Requirements for the Degree

Master of Science

By

Minyoung Jo

August 2013

Incorporation of Benzobisoxazole Cruciforms into Metal-Organic Frameworks and the Development of Fluoride Sensors Based on Benzobisoxazole Cruciforms

_____

Minyoung Jo

APPROVED:

_____

Dr. Ognjen Š. Miljanić, Chairman

_____

Dr. Scott R. Gilbertson

_____

Dr. Chengzhi Cai

_____

Dr. Ding-Shyue Yang

_____

Dr. Jeffrey D. Rimer

_____

Dean, College of Natural Sciences and Mathematics

ACKNOWLEDGMENTS

I first would like to express my deepest appreciation to Dr. Miljanić, my advisor, for his guidance, generosity, and support to complete my work. He has encouraged me to find the better way, and not only pushed me to achieve good results, but also lavished praise on improvement. I remember that his room was always open to listen to or discuss with us, and that is why other friends envied me. I also have been inspired by his passion for the research, and that has driven me to continue my academic career.

Additionally, I would like to thank Dr. Gilbertson, Dr. Cai, Dr. Yang, and Dr. Rimer for their precise time to serve on my master thesis committee.

I am grateful to Dr. Carrasquillo, Dr. Daugulis, Dr. Guloy, Dr. Jacobson, Dr. Cai, and Dr. May for the valuable lessons they provide me. I could acquire a great deal of knowledge of organic, inorganic, and physical chemistry in their classes.

I also express my gratitude to my undergraduate advisor, Prof. Il-wun Shim at Chung-Ang University. He still gives me a good advice about not only academic things, but also life.

I would like to thank all my past and current group members: Dr. Jaebum Lim (my mentor in cruciform synthesis), Teng-Hao Chen (another mentor in MOFs), Rio Carlo Lirag (the most humorous guy I have ever met), Qing Ji (the most gentle guy), Ha

Le (only one girl labmate who shared the laughs and the tears), Chia-Wei Hsu (a kind and friendly guy), Maxim Paci (“Mustard Pants”), and Xiao Liang (“J-star”).

I especially appreciate my husband, Seung Soo Lee, for his support, patience, and never-ending love. Although he was also busy, stressful, and tired, he never showed it outside. He makes me smile all the time and encourages me to do my best. Without him, the beginning of my journey for chemistry life might never been possible. My two cats (Choco and Mimi) made me feel less homesick and comfortable to focus more on my work.

I would like to say thank you to all my Korean friends at University of Houston: Dahye Lee, Soojeong Kim, Hana Lee, Donghyun Koo, and Hanju Lee. Especially I would like to tell Dr. Cho (Minjung Cho)—my first and best friend in Houston—that I will remember every moment we shared and miss you a lot.

At this moment, I want recall old faces in Korea to my mind: Sueyeon Hong, Jaemin An, Yujung Choi, Seunghui Ham, Yumi Kim, Mikyung Bae, Sungeun Park, and Eunju Lee. I cannot express how much I miss you, girls.

Last but not least, I would like to thank my mom, dad, brother, sister-in-law (brother's wife), and niece for their unconditional love showered on me. I will hug and tell them "I love you more than words can express" when we will get together again.

Incorporation of Benzobisoxazole Cruciforms into Metal-Organic Frameworks

and the Development of Fluoride Sensors Based on Benzobisoxazole Cruciforms

---

A Thesis Presented to

the Faculty of the Department of Chemistry

University of Houston

In Partial Fulfillment

of the Requirements for the Degree

Master of Science

By

Minyoung Jo

August 2013

ABSTRACT

Fully π-conjugated cross-shaped molecules known as molecular cruciforms have been studied for applications as versatile fluorescence sensors because they are characterized by spatially isolated frontier molecular orbitals, and thus a highly modular HOMO–LUMO gap leads to unique electronic and optical properties. In previous studies, benzobisoxazole-centered cruciform molecules with diverse substitution were developed, and these showed potential applications as chemosensory materials for numerous analytes. Based on the previous findings, solid-state sensors utilizing benzobisoxazole cruciforms which incorporated into porous crystalline materials, so called metal-organic frameworks (MOFs), through their coordination to transition metals were explored. A crystal structure of the first MOF incorporating a benzobisoxazole cruciform demonstrated the potential for rigid and strong optical solid-state materials where analytes could be transferred to the interior binding site on cruciforms through lots of pores of frameworks. An alternative synthetic method for our benzobisoxazole-bearing cruciforms was also suggested to achieve the large-scale preparation in enhanced yield. In addition, a new class of silyl alkyne cruciform which acts as sensitive and selective sensors for fluoride has been developed. The computational and spectroscopic studies revealed that these silylated benzobisoxazole cruciforms responded specifically to fluoride resulted from the desilylation of silylated alkynes while other anions did not make any chemical and optical changes.

TABLE OF CONTENTS

ABBREVIATIONS AND ACRONYMS

1D	one-dimensional
2D	two-dimensional
3D	three-dimensional
BDC	1,4-benzenedicarboxylate (terephthalate)
BPDC	4,4′-bipyridine dicarboxylic acid
BPY	4,4′-bipyridine
DEF	*N*-*N*′-diethylformamide
i-Pr_2NH	diisopropylamine
DMA	*N*,*N*′-dimethylacetamide
DMF	*N*,*N*′-dimethylformamide
DMSO	dimethylsulfoxide
DPNI	*N*-*N*′-di-(4-pyridyl)-1,4,5,8-naphthalene tetracarboxydiimide
ESI-MS	electrospray ionization-mass spectrometry
Et_3N	triethylamine
Et_2O	diethyl ether

EtOH	ethanol
FMO	frontier molecular orbital
HOMO	highest occupied molecular orbital
IR	infrared
LRMS	low resolution mass spectrometry
LUMO	lowest unoccupied molecular orbital
MeCN	acetonitrile
MeOH	methanol
MOF	metal-organic framework
NMR	nuclear magnetic resonance
PPA	polyphosphoric acid
SBUs	secondary building units
*t*Bu	*tert*-butyl
THF	tetrahydrofuran
TIPS	triisopropylsilyl
TLC	thin layer chromatography
TMS	trimethylsilyl

UV/Vis	Ultraviolet/Visible
ZIFs	zeolitic imidazole frameworks

Chapter One

Introduction to Cross-conjugated Molecular Cruciforms and Metal-Organic Frameworks

1.1 Molecular Cruciforms: Cross-conjugated π-electron Systems

In organic chemistry π-conjugated systems[1] typically refer to the connection of single and double (or multiple) bonds in an alternant fashion, which means that double bonds are not placed directly next to each other, but rather separated by a single bond. Partial overlap of *p*-orbitals on adjacent atoms enables delocalization of π-electrons through the whole conjugated system. It also contributes to lowering the overall energy, so consequently molecules with conjugated double bonds have higher stability compared to their isomers with isolated double bonds. Numerous organic molecules, from simple dienes and small aromatics to extended systems including graphene and carbon nanotubes, are all characterized by the conjugated system which delivers unique properties due to the broad delocalization of π-electrons as well as the flexible electron transfer along sp^2-hybridized systems. Special electronic properties of conjugated systems can be utilized in the construction of conductive materials, such as pentacene[2] and graphene.[3] In addition, conjugated systems have predictable optical properties, resulting in diverse colors that are useful in the design of synthetic dyes and organic pigments.[4]

To understand and predict the optical and electronic properties of conjugated π-systems, it is often not necessary to consider all of their molecular orbitals. Instead, more rapid insight into the unique features of conjugated systems can be obtained by simply examining their frontier molecular orbitals (FMOs): the highest occupied molecular

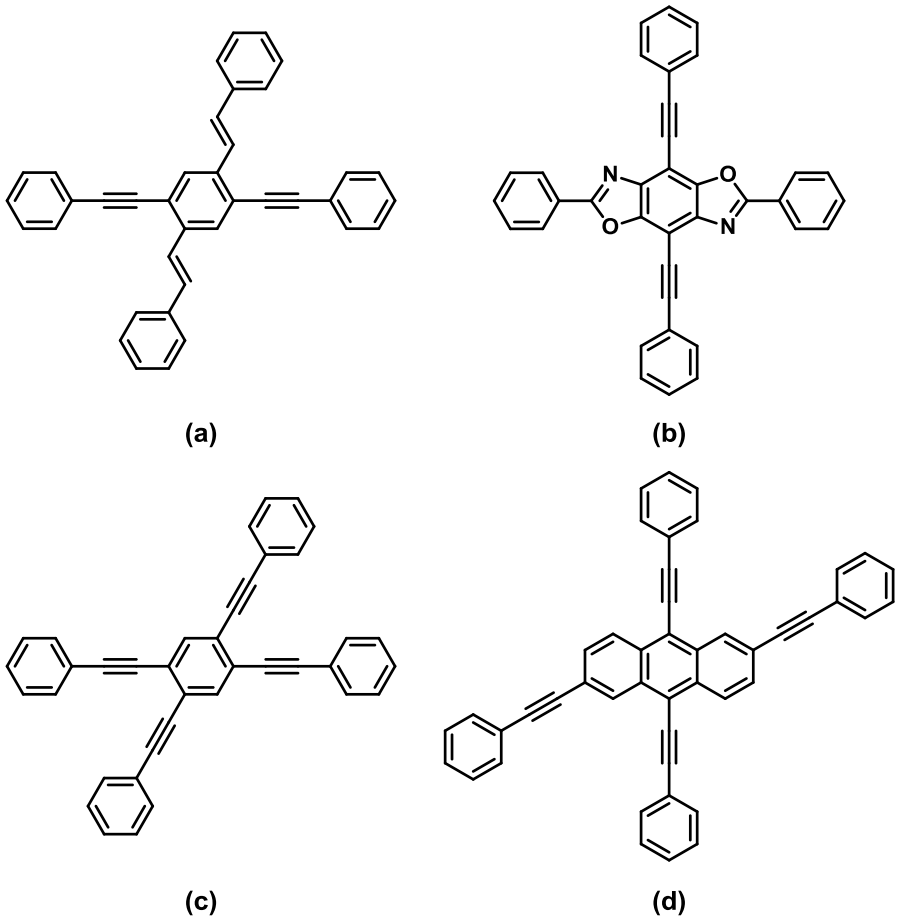

Figure 1.1 Representative examples of conjugated molecular cruciforms. (a) 1,4-distyryl-2,5-bisphenylethynylbenzene, (b) 2,6-diphenyl-4,8-dibromobenzo[1,2-*d*;4,5-*d*′]bisoxazole, (c) 1,2,4,5-tetrakis(phenylethynyl)benzene, (d) 2,2′-[[9,10-bis(2-phenylethynyl)-2,6-anthracenediyl]di-1,2-ethynediyl]bis[5-hexylthiophene].

orbital (HOMO) and the lowest unoccupied molecular orbital (LUMO). In most cases, the energy gap between the HOMO and the LUMO determines the reactivity and the optoelectronicet properties of the materials based on the conjugated molecules, which is of direct relevance to the applications of these molecules in areas that include organic light-emitting diodes (OLEDs),[5] field-effect transistors (FETs),[6] solar cells,[7] and chemical sensors.[8]

For easier modulation of HOMO and LUMO in conjugated systems, several classes of X-shaped "molecular cruciforms" have been developed recently, with examples shown in Figure 1.1.[9] This broad class of two-dimensional cross-conjugated molecules is composed of a central core to which four directional "arms" are attached. To ensure full conjugation across the molecule, the core part usually includes one or more (hetero)aromatic rings, and this core part connects to the arms of the cruciform through carbon–carbon double or triple bonds. In other words, two perpendicular π-conjugated circuits intersect at a central core. Functional groups can be placed at the end of each arm, which act as reactive sites that can engage in molecular recognition events or as anchors for immobilization of cruciforms on metal surfaces. Due to such a unique geometry, it is possible to easily control HOMO and LUMO in a cruciform molecule through the manipulation of substituents at the end of each arm. Typically, the separation of HOMO and LUMO can be tuned by adding either a donor or an acceptor substituent onto suitable end positions. Variety of cross-shaped conjugated materials have been synthesized, including spiro compounds,[10] paracyclophanes,[11] swivel-type dimers,[12] tetraethynylethenes,[13] and tetrasubstituted tolanes.[14]

The majority of studies of cruciform molecules have focused on the design of organic fluorophores for the construction of optoelectronic devices. Electronic substitution of this cross-conjugated scaffold tunes both the energy levels of HOMO and LUMO and their spatial distribution in cruciforms. The resulting fluorophores exhibit spatially isolated HOMOs and LUMOs, and are thus equipped with highly modular HOMO–LUMO gaps, of interest in sensory and other optoelectronic applications. Several

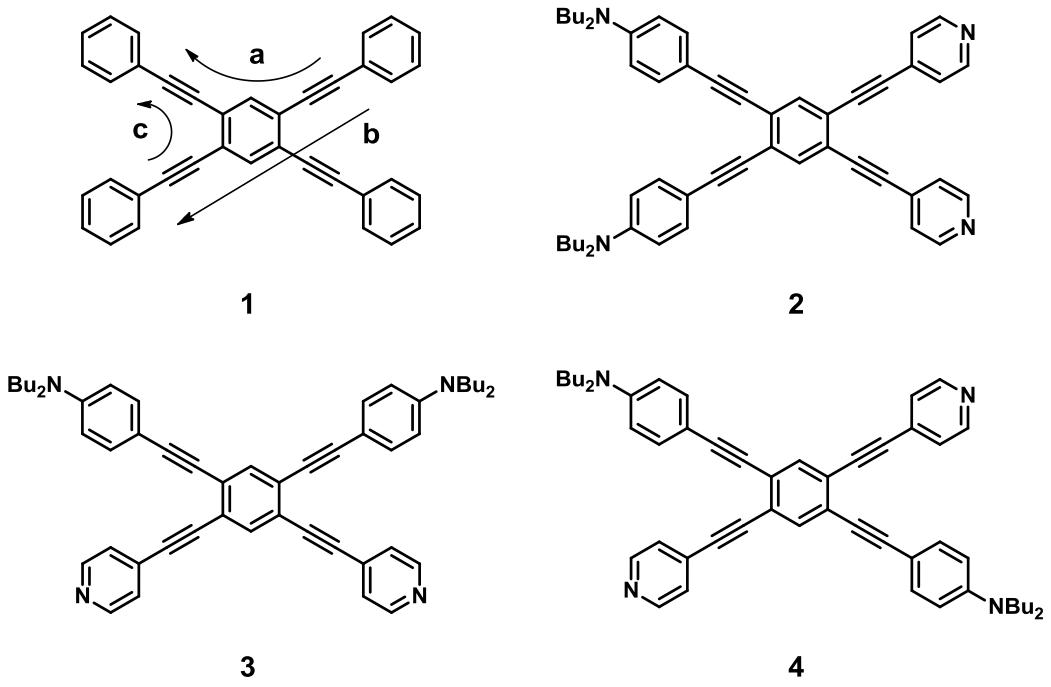

Figure 1.2 (1) Three types of charge-transfer conjugated pathways shown by arrows in tetrakis(phenylethynyl)benzene. Crossed pathway, horizontally linear pathway, and vertically bent pathway represent respectively arrow a, b, and c. Isomeric compounds of 1,2-bis[(4′-*N*,*N*-dibutylaminophenyl)ethynyl]-4,5-bis(2-pyridylethynyl)benzene; (**2**) pseudo*ortho*, (**3**) pseudo*meta*, and (**4**) pseudo*para* donor-acceptor substituted isomers.

investigators have explored cruciform π-systems, including Haley,[9b, 15] Bunz,[9a, 16] and Miljanić groups,[9c, 17] who respectively studies 1,2,4,5-tetraethynylbenzenes, 1,4-distyryl-2,5-bis(arylethynyl)benzenes, and 2,6-diaryl-4,8-bis(arylethynyl)benzobisoxazoles.

One of the significant cruciform molecule categories are the tetrakis(arylethynyl)benzenes that were studied by Haley and colleagues.[9b, 15] In particular, donor/acceptor-substituted tetrakis(phenylethynyl)benzenes exhibit a high degree of conjugation, and consequently possess multiple pathways for intramolecular electronic and photonic transfer (**1** in Figure 1.2).[15h] Their study focused on the structure-property relationships with specific structural modifications including placement of donor-acceptor substitution in *pseudoortho, pseudometa, and pseudopara* positions of the cruciform geometry as illustrated in Figure 1.2 (**2**, **3**, and **4**). Upon the understanding of mixed donor-acceptor systems that showed larger bathochromic shifts in the absorption compared to neutral or all-donor substituted cruciforms due to the charge transfer from the donor to the acceptor for the HOMO–LUMO transition,[15d] they revealed that the linear-conjugated pathways between donor and acceptor groups typically have distinct low energy band in absorption spectra, but cross-conjugated and bent-conjugated pathways (offered in *pseudopara* isomers) result in emission bands at longer wavelengths than linear ways.

Haley and coworkers also developed pyridyl-substituted systems based on the general tetraethynylbenzene cruciform motif, and have used these molecules for fluorescent sensing for metal ions.[15i] The metal ion–cruciform complexation upon the addition of Zn, Al, and Ag resulted in considerable red or blue shifts in the emission

spectra depending on their pyridyl substitution patterns (whether using 2, 3, or 4 pyridine as well as placing two acceptors in meta, ortho, or para position). The substitution of inductively electron-accepting $–CF_3$ groups (exemplified in Figure 1.3 as compound **5**),[15h] also gave their main scaffolds the equivalent optical behavior to nitrile or nitro resonance acceptors including distinct optical absorption and emission responses, high quantum yields, and significant red shifts according to decrease in band gaps. Additionally, the series of bis(dehydrobenzoannuleno)benzene[15b, 15h] including compound **6** that are locked into planarity by a diacetylene linkage were synthesized and examined the effects of improved planarization compared to original nonplanar cruciforms possessing the free rotation about the phenyl–ethynyl bonds. These molecules displayed relatively greater stability, smaller optical band gaps, and thus distinguished optical absorption and emission due to enhanced overall conjugation.

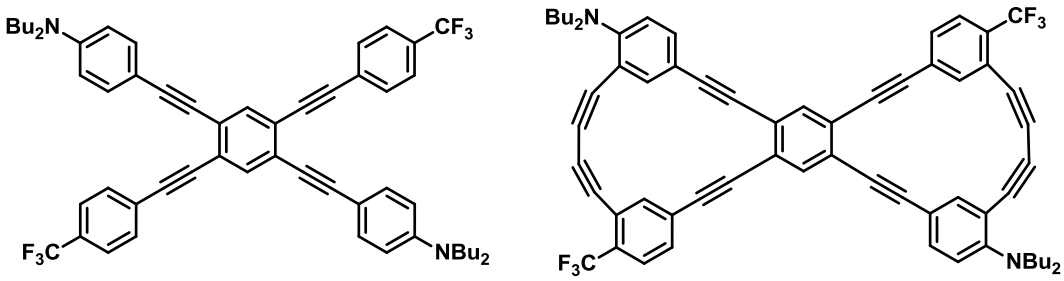

5 **6**

Figure 1.3 Haley's tetraethynylbenzene cruciform derivatives; benzotrifluoride-substituted compound (**5**) and bis(dehydrobenzoannuleno)benzene (**6**).

Bunz and coworkers have studied fluorescent sensors based on 1,4-distyryl-2,5-bis(arylethynyl)benzenes (as shown in Figure 1.4).[9a, 16] Unlike Haley's cruciforms, more electron-rich distyryl connection was introduced for one axis instead of ethynyl group. In most of their donor/acceptor combined systems, electron-donating substituents are located on this electron-richer distyrylbenzene axis, and electron-accepting substituents are attached to the ethynyl axis to magnify the intrinsic electronic characteristics of the substituents. The analysis of the electronic structures of the derived cruciforms showed that—like in the preceding case—the terminal substitution plays a vital role to determine where the HOMO and LUMO are located, whether they are spatially separate from one another by localizing on the orthogonal arms of the cruciforms, as well as what kind of analytes they recognize. Some representative Bunz's cruciform products (Figure 1.4) and the brief explanations on their sensory performances were described as follows. They investigated the responses of spectroscopic properties of compound **7**[16s] to Lewis acidic metal cations (Mg^{2+}, Ca^{2+}, Mn^{2+}, and Zn^{2+}). The Lewis basic end groups on each branch (dimethylamino or pyridyl) provided a handle for analyte recognition, and their electronic properties also promoted the spatially isolated arrangement of the FMOs. In this cruciform, the HOMO is localized along the axis substituted with strongly electron donating dialkylaniline groups, while LUMO resides along the axis holding electron-accepting pyridyl groups. Therefore, it is possible that binding of a positive ion to the aniline branch, where the HOMO resides, leads to a stabilization of the HOMO, but leaves the LUMO unchanged, thus increasing the size of the HOMO–LUMO gap causing blue shifts in both absorption and emission. Exposure of other cruciforms such as compound **8**,[16f] and **9**[16k] to metal salts also induces strong response in absorption and

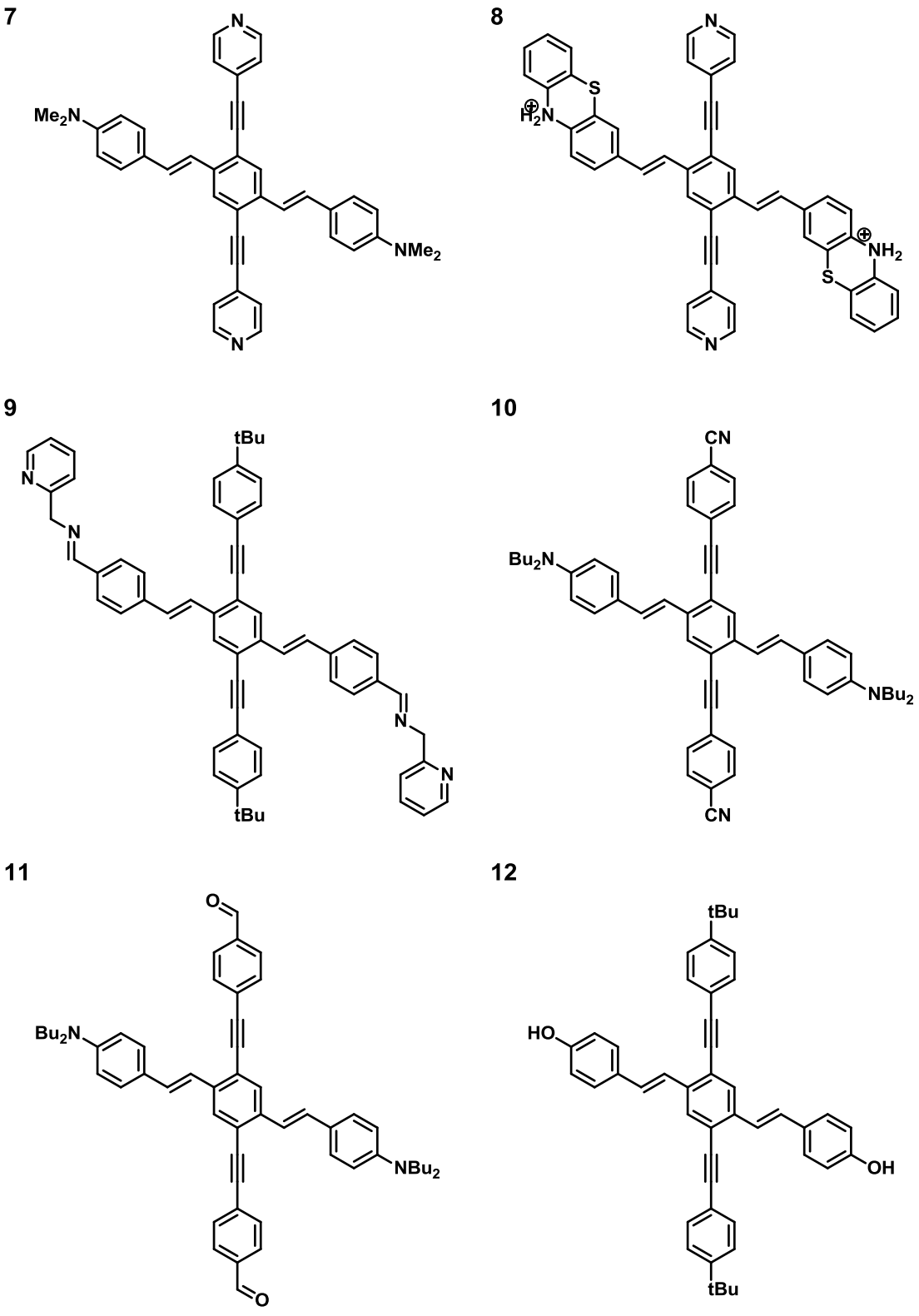

Figure 1.4 Representative 1,4-distyryl-2,5-bis(arylethynyl)benzene cruciforms.

emission. Compound **8** contains phenothiazine terminals on the arylenevinyl axis and shows large metallochromic effects toward several metal ions because phenothiazine is easily oxidized with several redox-active metals. Compound **9** includes imine moiety, which displays attractive binding to Cu^{2+} and Zn^{2+} and stabilization of only LUMO by metal binding. Compound **10**[16b] can discern different carboxylic acids that have close pK_a values from each other (with great selectivity), and compound **11**[16j] decorated with aldehyde groups along the ethynyl branch is used for primary and secondary amine sensing, demonstrating appealing fluorescence turn-on behavior upon detection of analyte amines. In addition, their attempts extended to a class of conjugated polymers, where some cruciforms were prepared to obtain poly(*para*-phenylenevinylene)s for the application toward new organic sensing devices.[16p] Bunz group has also developed a wide range of other cruciforms including hydroxyl-substituted systems (**12**)[16g, h] for amine-sensing, water-soluble molecules[16l, 16n] for the analysis of the coordination of metal ions at different pH, fluoride-sensing cruciform materials,[16a] unsymmetrical cruciforms,[16m] as well as the fluorophore arrays combining three cruciforms for efficient discrimination of carboxylic acids.[16b]

Benzobisoxazole-based cruciforms were pioneered by Nuckolls[18] and have been subsequently used by several other groups,[9c, 17-19] including ours. Nuckolls and co-workers have prepared cruciform π-systems in which a conjugated and horizontally situated benzobisoxazole branch intersects with a vertically positioned terphenyl arm at the central heterocyclic benzobisoxazole ring. Benzobisoxazoles have near-planar structure which can facilitate efficient packing and charge transport in addition to four available valences for the placement of various substituents at a regular 90 ° angle. Their

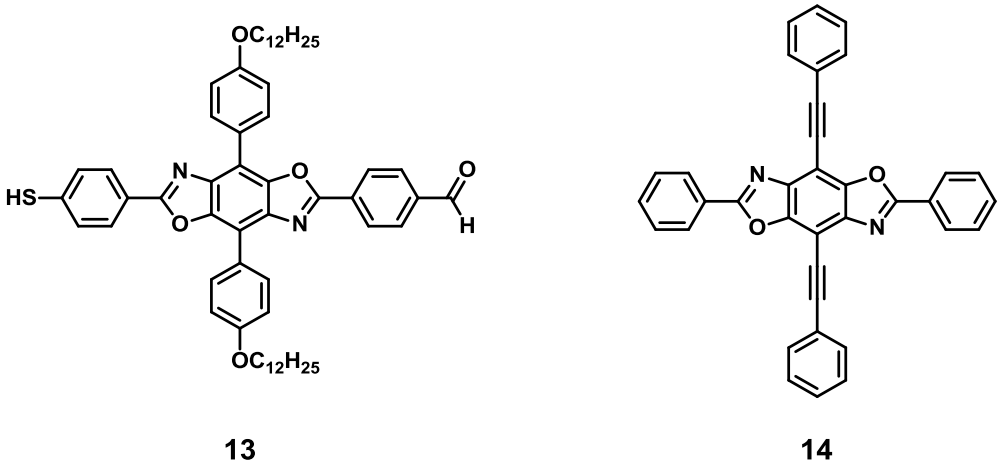

Figure 1.5 Benzobisoxazole cruciforms studied by Nuckolls (**13**) and Miljanić (**14**).

study has focused on the use of cruciforms in molecular electronics, wherein linear conjugated path is required to interface with the metallic electrode surface. The cruciforms provided not only the conjugation pathways, but also a coordination site to thin films with another orthogonal arm. Nuckolls' cruciform molecules based on the benzobisoxazole core were applied for the assembly of ordered monolayer films, where the bisoxazole subunits are attached through thiols or nitrile and placed upright on a metal surface. The path of conjugation on the film can be extended through imine formation between aldehyde-functionalized cruciform monolayers (Figure 1.5, **13**) and a variety of anilines.[18b] From this work, they showed that the introduction of conjugated cruciform with the structural advantage to self-assembled monolayers (SAMs) can create promising molecular-scale electronic devices.

In the Miljanić group,[9c, 17] benzobisoxazole cruciforms were explored as a new class of fluorescent sensors capable of detecting a wide variety of analytes. Recently, Miljanić and coworkers reported several heterocyclic cruciform derivatives with central benzobisoxazole nucleus which feature two aryl horizontal arms and two vertical arylethynyl arms located in the orthogonal way (Figure 1.5, **14**). Localization of HOMO and LUMO in these cruciform conjugated systems at the different arms was completed depending on the end-functional groups and suggested promising sensing properties in response to numerous analytes, such as carboxylic and organoboronic acids, phenols, amines, ureas, and several small organic and inorganic anions.[17a, b] Moreover, unlike Bunz and Haley's cruciforms sets, benzobisoxazole-based systems provide almost 90^{o} angle of products which is unique geometry applicable for solid-state extended frameworks as well as additional potential recognition sites with the nitrogen and oxygen atoms on the core.

1.2 Introduction to Metal-Organic Frameworks (MOFs)

Within the last two decades, microporous materials constructed from transition metal clusters and bridging organic ligands, commonly known as metal-organic frameworks (MOFs), have been at the center of a rapidly growing field.[20] An explosion of interest in these inorganic hybrid materials comes from their proven viability as platforms for numerous applications, including gas storage[21] and separations,[22] heterogeneous catalysis,[23] ion-exchange,[24] drug delivery,[25] luminescent materials for sensing,[26] organic magnets,[27] and biomedical imaging.[28]

The term MOF was first coined in 1995 by Yaghi for a layered cobalt-benzenetricarboxylate framework that showed reversible sorption properties towards aromatic guest molecules.[29] Three-dimensional (3D) MOFs were introduced by Kitagawa and Yaghi in 1997; Kitagawa reported bipyridyl bridging structure with cobalt, nickel, and zinc, which exhibited gas sorption properties at room temperature,[30] while Yaghi reported MOF-4, a zinc-benzentricarboxylate network that showed rigidity and stability even in the absence of solvent guest molecules.[31] The seminal discovery of MOF-5 in late 1990's introduced this 3D framework material with unprecedented high surface area, permanent porosity, and high thermal stability. MOF-5 is composed of the zinc oxocarboxylate cluster in which a central Zn_4O tetrahedral unit coordinates to six carboxylate groups into a cluster shaped like a regular octahedron (Figure 1.6).[32] Propagation of these octahedral clusters in three dimensions is achieved through their cross-linking via benzenedicarboxylate (terephthalate) ligands. Thus far, several hundred different MOFs have been identified, and this is only a small portion of conceivable

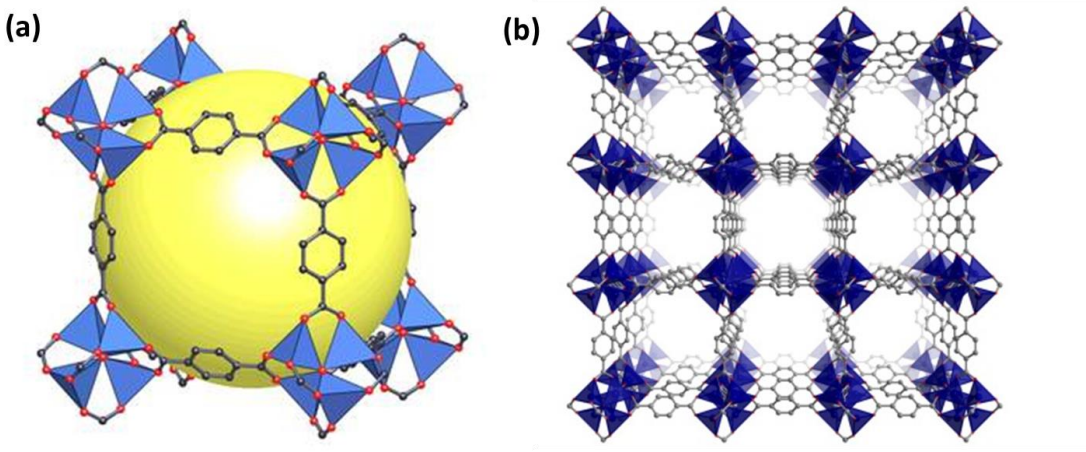

Figure 1.6 Crystal structure of MOF-5. Zn_4O units are presented as blue polyhedra bridged by benzene dicarboxylate linkers. Oxygen and carbon are illustrated by red and back spheres respectively. A yellow ball indicates a large cavity in the framework. (b) Packing diagram of MOF-5 shows infinite three-diminsional nerwork.

materials because of the huge variety of possible linkers and inorganic units as well as the potential to postsynthetically tailored MOFs.[33]

MOFs are often compared to conventional porous materials, such as zeolites and activated carbons. However, zeolites and other purely inorganic crystalline solids mostly suffer from lack of structural diversity and functional tunability, whereas organic porous solids like activated carbon are amorphous or at best partially ordered in a crystallographic sense. In contrast, MOFs represent highly ordered organic-inorganic hybrid frameworks, which combine immense structural diversity—owing to their modular synthesis, with crystallographic order that allows atomic-level interpretations of

their structures and functions.[34] Other desirable properties of MOFs include high thermal (although often not chemical) stability, high surface areas, and permanent porosity.

MOFs consist of two major components: inorganic metal ion clusters and organic molecular linkers. Inorganic subunits can be constructed from essentially any metal in the periodic table, while organic units typically utilize oligodentate ligands, with some examples shown in Figure 1.7. This variety of metal ions, organic linkers, and structural topologies leads to essentially an infinite number of possible combinations with diverse properties. This geometry, as well as individual properties of metals and organic linkers dictates the MOFs' properties that form the basis of their applications. Majority of organic ligands are the carboxylic acids and dipyridyl compounds. Carboxylates favor the formation of chelate with metal ions to easily lead metal-oxygen-carbon clusters, and also provide the potential extended structure relying on the type of carbon moieties of carboxylates. In addition, the presence of strong metal-oxygen bonds provides the robustness and stability of the assembly.[20f, g, 35] Metal-pyridine linkage also has been widely employed in coordination polymers, which is generally not stabilized against channel collapse, so that the mixed-coordination approach combining carboxyl and pyridyl ligands (such as in pyridine-pillared tetracarboxylate paddle-wheel structures) is proposed to give much greater variety of topologies and properties.[36] Special kinds of MOFs, so called ZIFs (zeolitic imidazole frameworks), are derived via binding metals to nitrogens of imidazolate where strong Zn–N bonds offer exceptional chemical and thermal stability.[37] The defined geometrical shapes affording directionality and rigidity in MOFs referred to as secondary building units (SBUs),[38] which enable the prediction of

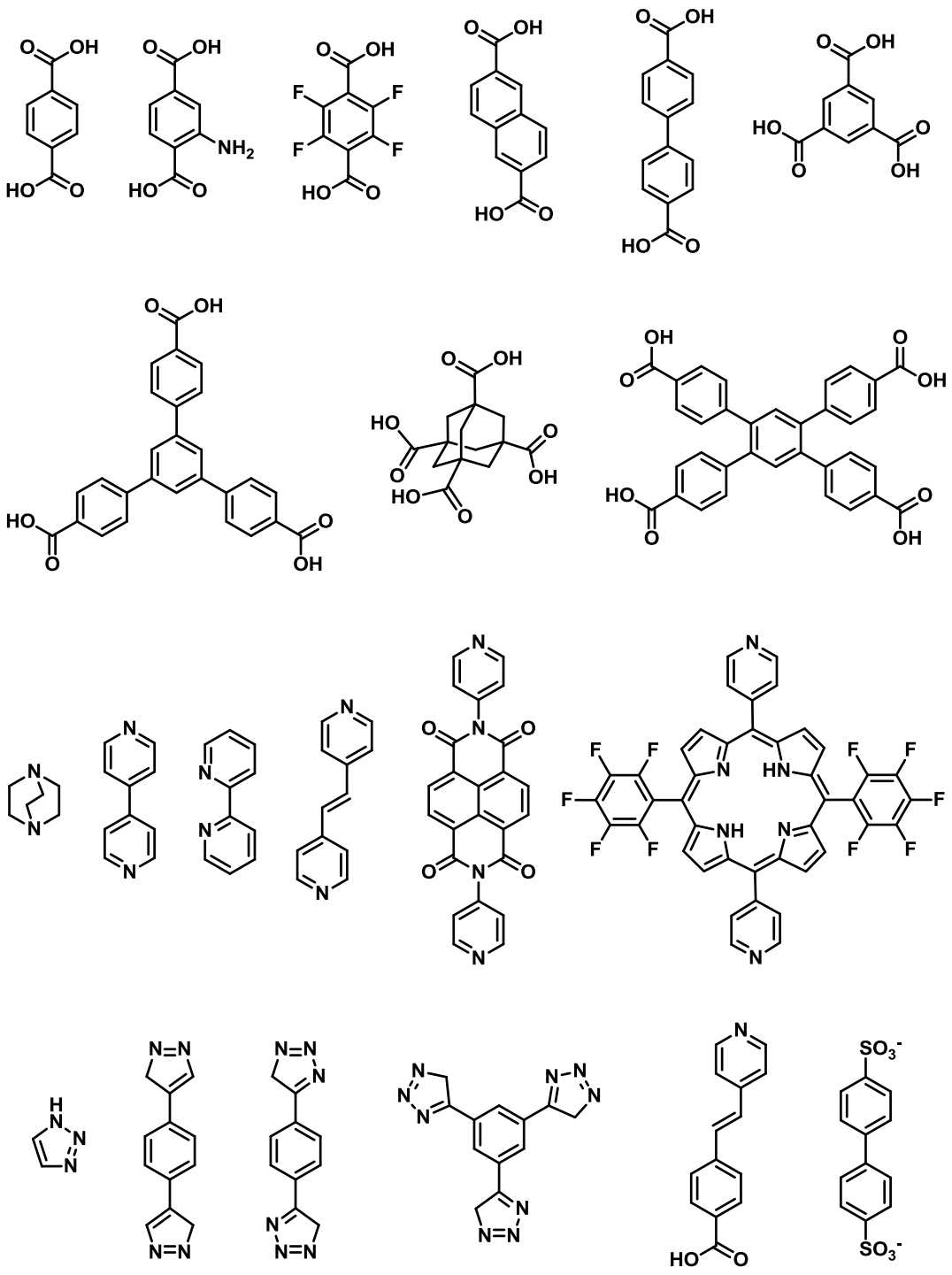

Figure 1.7 Library of commonly used organic ligands in the syntheses of MOFs.

the topologies of new complex and allow the design of highly porous and robust MOF structures as desired.

The knowledge of possible topologies, the functionality of multitopic organic linker molecules, as well as the understanding of typical metal coordination environments or the formation conditions of typical inorganic building blocks help one to understand and direct the synthesis efforts. The essential strategy of MOF synthesis is to establish the synthesis conditions that afford well-defined inorganic building blocks without decomposition of the organic linker. Besides, the kinetics of crystallization must be controlled, so that the single crystalline samples can be obtained (and subsequently characterized by X-ray crystallography). The resulting MOFs are strongly influenced by compositional (molar ratios of starting materials, pH, solvent, etc.) and process parameters (reaction time, temperature, and pressure), which yield different particle sizes and morphologies of MOFs, and thus the formation of MOFs necessitates the application of different synthesis methods. Conventional synthetic strategy has been widely used under solvo/hydro-thermal conditions, in which reactions take place in closed vessels under high vapor pressure, usually close to or above the boiling point of the solvent. Other method also have been proposed, including microwave-assisted methods,[39] microfluidics,[40] aerosol,[41] mechano-,[42] sono-,[43] and electro-chemical synthesis.[44]

Postsynthetic modification of MOFs[45] is another emerging method to manipulate the framework directly, in most cases, by conducting the organic reaction on the potential reactive site of organic linking component of MOFs. Accordingly, the original MOF turns into a new MOF with the generation of new functionality, and thus different

physical and chemical properties. Post-synthetic coordination of additional metal ions to sites on the bridging ligands[46] and addition/removal of metal atoms to the metal site[47] have been explored as well.

As previously touched on their characteristics, MOFs are primarily characterized by permanent high porosity that allows guest molecules to diffuse into the void space of the structure. In addition, the shape and size of pores determine the selectivity of guest recognition, which also occurred without collapsing or any changes on properties. Interestingly, unlike other solid matter, such as zeolites, carbons and metal oxides, large numbers of these coordination polymers exhibit high framework flexibility–shrinkage/expansion caused by interactions with guest molecules.[20d] Unlimited possibilities for modification and delicately tuning their structures and properties are also important attractive advantages for MOFs that rely on the choice of metal-containing SBUs and bridging linkers. Although high surface areas are already found in activated carbons and zeolites, MOFs are far superior in this regard: for example, in the case of MOF-177, surface area reaches 5640 m^2g^{-1},[48] and for MIL-101 it goes up to 5900 m^2g^{-1}.[49] MOFs are also highly thermally stable materials, typically resisting decomposition at temperatures up to 300 ºC, and sometimes as high as 500 ºC.[50]

Variability for the organic and inorganic components permits these sophisticated architectures to have numerous potential applications. These include the more traditional areas of gas storage, separation, and catalysis, which are based on the pore size and shape as well as host–guest interactions involved. The design of gas storage targeting, mostly, hydrogen,[21b, 21e, 21i, j] and methane gases[21c, 21f] has been developed so that many MOFs

show high adsorption capacities on the specific gas. The potential CO_2 capture adsorbents[21c, 21g, h] using the highest surface area have been proposed as next-generation materials for carbon capture and storage. Selective separation of gases[22] surpassing conventional method like distillation is a promising prospect being currently explored. MOF-based enantioselective catalysis[23] is possible to assign diverse functional organic ligands in the structure. Further areas of intense investigation include the use of MOFs as sensory materials with the luminescent properties based on linkers, metals or guests,[26] magnetic property of MOFs,[27] as well as biomedical applications.[28]

1.3 Conclusion

Three representative cruciform series—tetrakis(arylethynyl)benzene, distyryl-bis(arylethynyl)benzenes, and diaryl-bis(arylethynyl)benzobisoxazoles—were addressed with their optical and electronic properties, as well as applications based on the terminal substitution on the arms of these cruciforms. Metal-organic frameworks are also introduced with their unique characteristics that include high porosity, large surface area, tunable functionality, and thermal stability in addition to the composition of the crystalline materials and their diverse potential applications. Chapter 2 of this thesis will describe our efforts to integrate benzobisoxazole-based cruciforms into metal-organic frameworks with the intention of obtaining well-defined solid-state fluorescent sensing materials. Subsequently, in Chapter 3, new benzobisoxazole sensors that use simple desilylation reaction with prominent selectivity and sensitivity towards fluoride will be presented.

Chapter Two

Incorporation of Molecular Cruciforms into the Metal-Organic Frameworks

2.1 Introduction

Metal-organic frameworks (MOFs) are a class of extended crystalline materials that typically feature extremely high porosity and large surface area. They are built from divergently positioned metal ions and organic bridging ligands, which together establish infinite network structure with inorganic units residing at vertices (nodes) of the frameworks and organic molecules connecting the inorganic cluster nodes as struts. Because of their structural rigidity, thermal stability, and functional versatility, the applications of these materials are expanding dramatically in diverse fields including gas storage and separation, catalysis, and sensing. When it comes to the construction of these coordination networks, the choice of metals and linkers has significant effects on the structures and properties of the MOFs. For instance, each metal has preferred coordination geometry with given organic ligands, dictating how many ligands can bind to it or what their relative orientation will be. It leads to the different size and shape of pores of MOFs, thus influencing their extended structure as well as functionality—the latter being most intimately connected to the framework's porosity and the functional properties of its organic molecular groups.

As described in Chapter 1, fully conjugated cruciform-shaped molecules (simply called cruciforms) show good sensing performance with a variety of analytes based on

their terminal substitution, which both dictates their HOMO/LUMO energy states and introduces binding sites for potential analytes. Typically, optical properties of a molecule can be rationalized based on their HOMO–LUMO gaps. Therfore, in the development of molecular sensors, one of the key issues is the ability to achieve separate control of HOMO and LUMO energies, in order to be able to predictably modulate the sensor's HOMO–LUMO gap upon its interaction with an analyte and induce recognizable optical responses.

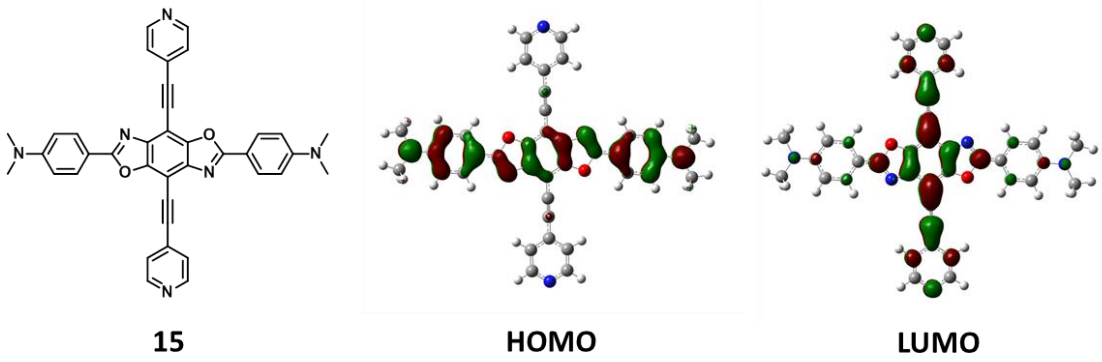

Figure 2.1 Cruciform **15** and computed orbital densities of HOMO and LUMO, calculated at the B3LYP/6-31G** level of theory.

One of our benzobisoxazole cruciforms **15** (Figure 2.1) was already identified as a good sensor for protons,[9c] carboxylic acids,[17b] phenols,[17b] amines,[17a] ureas,[17a] and anions.[17a] Cruciform **15** consists of two perpendicular and fully conjugated arms intersecting at a benzobisoxazole central core, wherein terminally amine-functionalized phenyl groups are located on the horizontal arm, and pyridine-substituted alkynes are attached to the core ring vertically. Computational study shows that HOMO of **15** is

localized along the donor-substituted horizontal axis, and its LUMO is localized along the electron-accepting vertical axis (Figure 2.1). This spatial separation of HOMO and LUMO contributes to the phenomenon that only the HOMO or the LUMO will be stabilized when binding of an analyte occurs at the corresponding site. Cruciform **15** has two different detection sites: aniline and pyridine which are both basic and thus prone to protonation. In the previous literature,[9c] the addition of trifluoroacetic acid to the solution of cruciform **15** allowed the pyridine sites to protonate first, thus stabilizing its LUMO without a significant change in the HOMO energy and causing a red (bathochromic) shift in absorption spectra. Upon continued addition of acid, proton binding also occurred at the dimethylaniline sites, and thus the absorption plots moved to the blue region again (hypsochromic shift), consistent with the stabilization of the HOMO.

Sensitive and selective detection of various analytes is required for a wide range of applications including industrial process management, chemical threat detection, medical diagnostics, food quality control, occupational safety, and environmental monitoring. While a variety of chemical sensors have been successfully generated and commercialized, improvement is still necessary for more stable, selective, and real-life materials targeting numerous analytes.[26b] We aimed at creating solid-state sensors utilizing our cruciform fluorophores that have been already proved as useful solution-phase sensors for various analytes because solid-state sensors hold greater promise in terms of portability and reversibility in device applications. Through the incorporation of cruciform sensors into MOFs, it was expected that their optical properties would readily translate from solution to the solid state, as the porous structure of the MOF was expected to both permit facile guest influx and to prevent problems associated with aggregation in

the solid state. Cruciform-shaped molecules are particularly good candidates for an organic linker in MOF structures. First of all, these fully conjugated cross-shaped molecules are rigid; their low flexibility is expected to enable them to maintain the structural integrity and crystallographic order within a MOF. In addition, the cruciform scaffold is linear, and two branches are crossing in the perpendicular fashion, which allows access to a plethora of well-defined networks derived from linear linkers. Finally, our cruciform **15** is already predispositioned to act as an analog of bipyridyl ligands for coordination with inorganic clusters, a structural motif that had been amply precedented in MOF chemistry.[36, 51] Meanwhile, amine-substituted arms remain free to be a potential site for molecular recognition and sensing. It is assumed that selective transfer of analyte inside the structure, depending on the size of pores, enhances binding of specific analytes (and prohibits binding of inappropriately sized analytes) to cruciforms, inducing strong optical changes. Regeneration of the sensors is also possible through the reversible uptake and release of guest substrates offered by the permanent porosity.

To the best of our knowledge, only one example of MOF that incorporated cross-shaped ligand was reported by Yaghi and co-workers in 2012.[52] In that work, a tetracarboxylate-substituted cruciform molecule was employed to provide four connections along the all branches to four different zirconium(IV) secondary building units, thus leaving no available sites for molecular recognition and/or sensing.

In the following section, the synthesis of two benzobisoxazole cruciforms (**15** and **16**) selected for incorporation into MOFs is described. Cruciform **16**, which has neutral phenyl-substituted arm horizontally, was chosen for the generation of framework prior to

cruciform **15**, in order to investigate the possibility of the incorporation of benzobisoxazole cruciforms into the 3D network. Moreover, cruciform **16** is somewhat easier to produce than compound **15**. For cruciform **15**, modification of previous procedure was required to readily generate this material in high yield on a large scale. The incorporation of these cruciforms into highly ordered porous materials was attempted and resulted in a previously unknown crystallographically characterized hybrid structure (**17**) between one of the molecular cruciforms and metal ions—suggesting a promising solid-state optical device.

2.2 Results and Discussion

2.2.1 Preparation of Cruciform Compounds as Precursors for MOF

Cruciform **16** was synthesized (Scheme 2.1) partially following the procedure from our group's previous publication.[9c] Starting from dihydroquinone (**18**), bromination affords bromanil (**19**), which is then subjected to nucleophilic substitution with ammonia in ethanol to afford compound **20**. A reduction reaction then produces material **21**. The horizontal axis of the cruciform is then established through a dehydrative condensation of **21** with benzoic acid into dibromobenzobisoxazole derivative **22**. Microwave-assisted Sonogashira coupling reaction of **22** with 4-ethynylpyridine (**29**)[53] successfully generated cruciform **16** in 31% yield. This cruciform compound was used for the synthesis of framework **17** described in the next subsection.

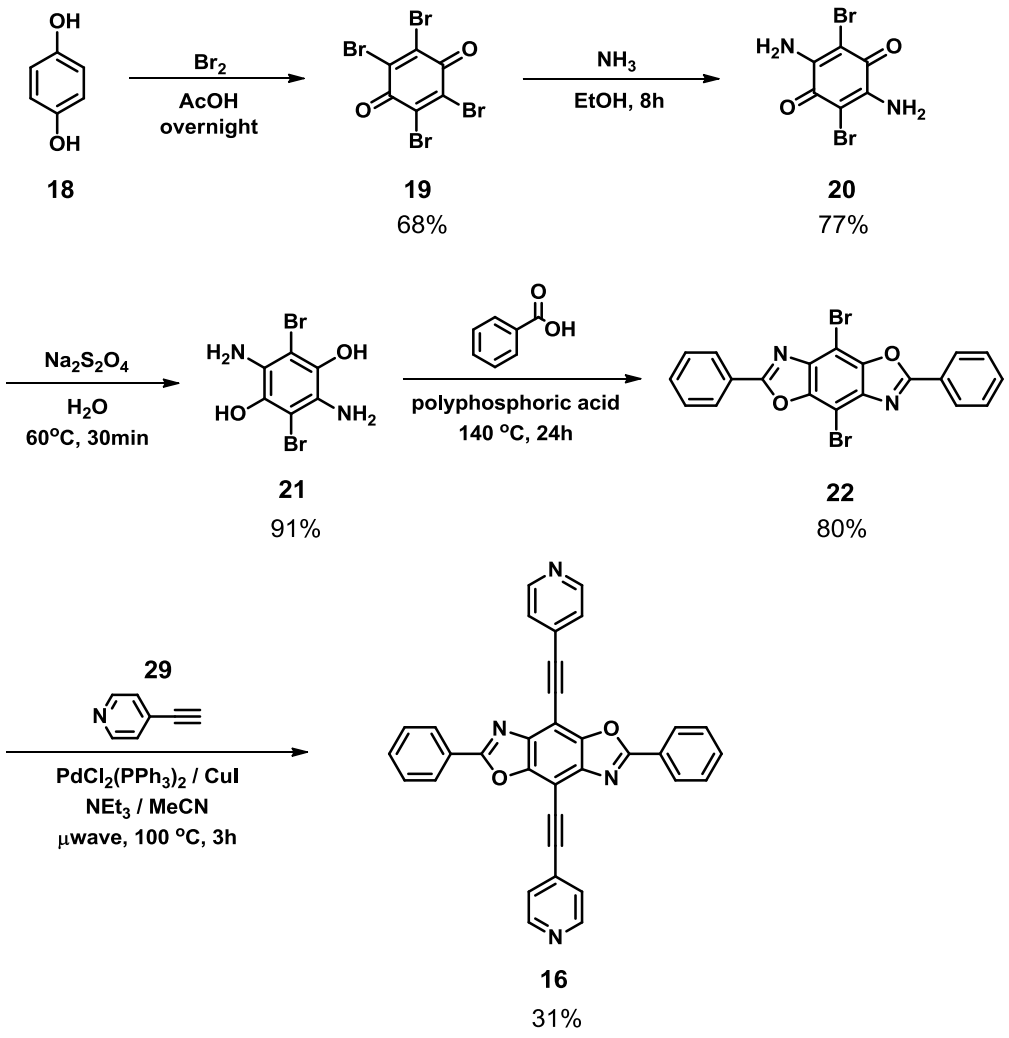

Scheme 2.1 Synthesis of cruciform **16**

Cruciform **15** was prepared by modifying previously reported procedure.[9c] Although the synthesis of cruciform **15** in moderate yield was already published, this route was problematic in producing larger amounts of this cruciform, which were needed to screen extensive sets of conditions for the synthesis of cruciform-based MOF. We traced this trouble back to the reproducible preparation of precursor 4-ethynylpyridine (**29**) on a large scale. The previous method (Scheme 2.2, upper-right procedure) utilized

this material, but we found that it was decomposed easily due to its susceptibility to light, thus making the final Sonogashira coupling step challenging. This issue was further exacerbated by the difficulties in the purification of the starting material—compound **23**, which was problematic because of its poor solubility in common organic solvents. In contrast, newly developed method (Scheme 2.2, lower-left route) includes first Sonogashira coupling reaction with trimethylsilylacetylene (TMSacetylene), followed by desilylation and then another coupling reaction with 4-bromopyridine. In the first stage,

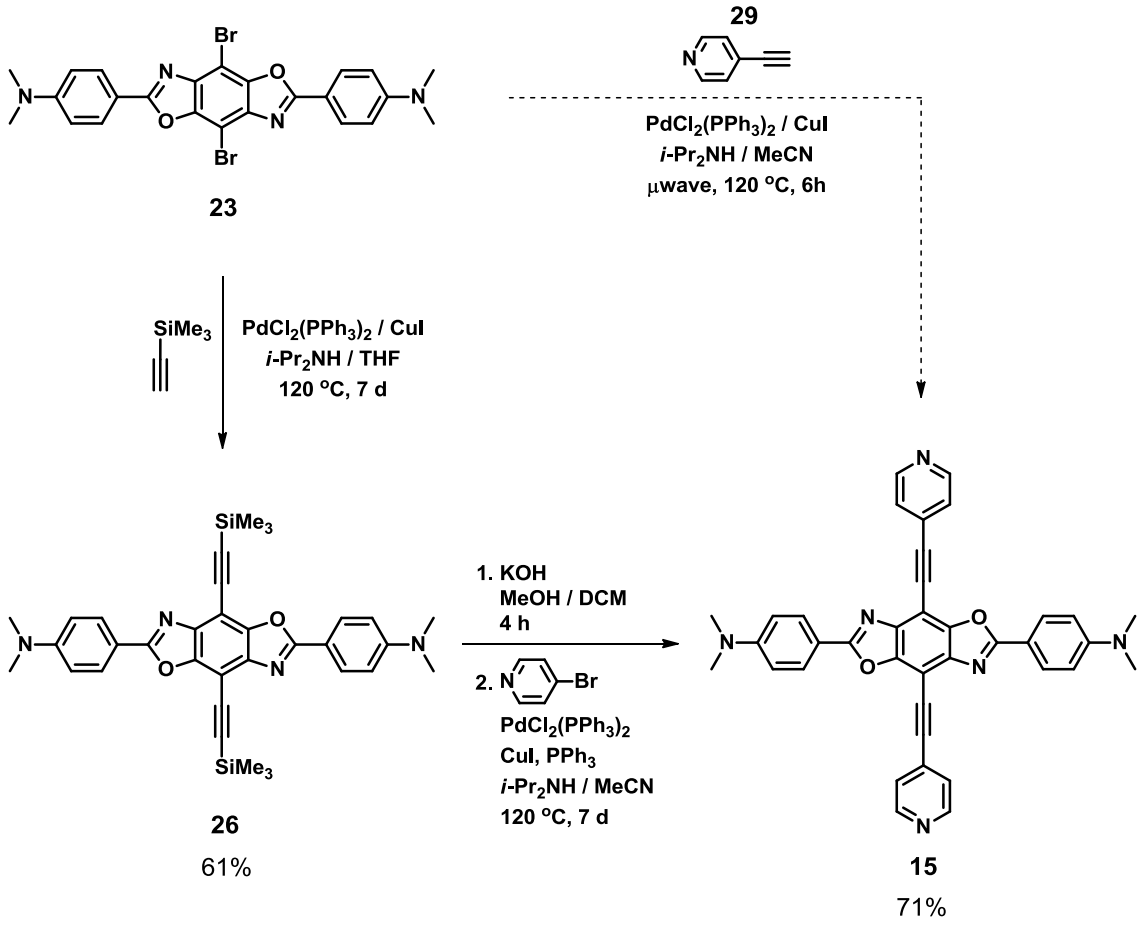

Scheme 2.2 Newly developed synthetic route to cruciform **15**.

cross-coupling reaction between TMSacetylene and aryl halide without the need for microwave assistance enables this reaction to proceed on a large scale. Furthermore, the silylated cruciform intermediate **26** is a convenient compound to handle since it exhibits high solubility in most organic solvents and stability without any decomposition. In spite of using crude benzobisoxazole reactant, pure product **26** was isolated in 61% yield after a single column chromatography. Following simple desilylation with KOH and Sonogashira coupling reaction with 4-bromopyridine was performed in 71% yield to give around 650 mg of cruciform **15**.

2.2.2 Synthesis of Cruciform-incorporating MOFs

Two representative MOF families were used as platforms for the incorporation of cruciforms into MOFs The first one is MOF-5, initially reported by Yaghi in 1999.[32] MOF-5 is assembled by the coordination of Zn(II) ion and terephthalic acid into a basic zinc oxoacetate structure. Two carboxylic group protons in each acid molecule were deprotonated by the base that was formed by high-temperature decomposition of diethylformamide (DEF), and thus these carboxylate anions were connected to Zn center forming octahedral secondary building unit (SBU), which then propagates into “infinite” cubic crystalline structure. The second motif we employed was MOF-508, also published by Yaghi,[54] which is composed of one metal unit and two organic molecules—one carboxylic and one pyridyl linker. In the Zn-based MOF-508 structure, the organizing motif was "capped paddle-wheel" binuclear Zn cluster, in which two Zn ions are bridged by four carboxylic groups into a paddle-wheel geometry, and then pillared through

bipyridyl groups that then bridge one cluster with the next, resulting in a pillared 3D architecture. Paddle-wheel unit is one of the most common inorganic building blocks in MOFs, and the large number of the compounds containing paddle-wheel units is based on Cu and Zn, but examples with other ions such as Mo,[55] Fe,[56] and Cr[57] were also reported.

In order to build robust 3D frameworks based on the cruciform motif, "pillaring" strategy illustrated in MOF-508 above was adopted through the replacement of the simple 4,4′-bipyridine with a cruciform-based bipyridine **16** in our proposal. Specifically, it was envisioned that the combination of cruciform **16** and linear dicarboxylic acids would result in a layered two-dimensional (2D) Zn-dicarboxylate structures, which would be connected to each other through cruciform linkers.

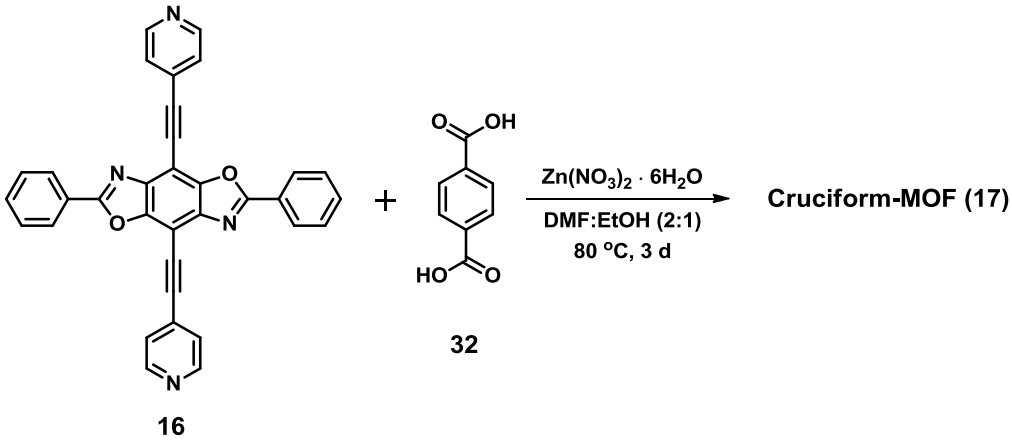

Scheme 2.3 Preparation of cruciform-MOF **17**.

To obtain the desired cruciform-based MOFs, a number of diverse reaction conditions were screened, with variable parameters that included temperature, reaction time, solvent composition, reactant concentration, and sometimes reaction vessel size.

Our first cruciform-bearing MOF was accomplished by solvothermal reaction, in which cruciform **16** and terephthalic acid (BDC) with $Zn(NO_3)_2 \cdot 6H_2O$ were heated in a mixture of *N*,*N*′-dimethylformamide (DMF) and ethanol (2:1) at 80 ℃ for 3 days produced the rod-shaped crystalline materials.

Despite extensive experimentation aimed at optimizing the yield of pure products, resulting solids from the solvothermal reaction were observed to be mixtures of the desired single crystalline material and other polycrystalline byproducts. In addition, unlike general organic molecular products, common purification methods such as distillation, recrystallization, or chromatography are not suitable for isolation of these organic-inorganic hybrid compounds. Interestingly, Hupp and Kepert[58] suggested separation techniques for rapidly purifying MOF materials, which use density differences between the mixture components to isolate them from each other through flotation. Brominated solvents were preferred for achievement of the appropriate density due to their high density relative to most MOFs. This simple method first suspends the crude MOF mixture in a dense solvent—on which all the components float, and then another lighter and miscible solvent is added so that the mixture separates into floating and sinking portions based on their respective densities. An important consideration, of course, is that solvents are not chemically reactive with MOFs, i.e. that they do not collapse or decompose the framework(s). We chose dibromomethane (CH_2Br_2) as the first solvent, whose density is 2.50 g cm^{-3}, and the desired density was reached while adding dichlromethane (CH_2Cl_2, 1.33 g cm^{-3}). At the beginning, all solids floated to the surface of pure CH_2Br_2 and addition of CH_2Cl_2 allowed undesired opaque materials to

sink. Floating crystalline materials were collected, and the procedure was repeated until only pure crystalline product could be obtained.

To determine the content of organic linkers in the obtained single crystalline product, a portion of this material was digested for further characterization using solution-phase NMR, according to the previous literature.[59] The resulting material was washed several times with fresh CH_2Cl_2 and soaked in CH_2Cl_2 for 3 days while exchanging with fresh CH_2Cl_2 on a daily basis. The solvent was removed by filtering and drying at 120 ℃ under vacuum over night. Dried crystals were then dissolved in 0.1% DCl solution in DMSO-d_6. This digestion solution was used directly for ^{1}H NMR.

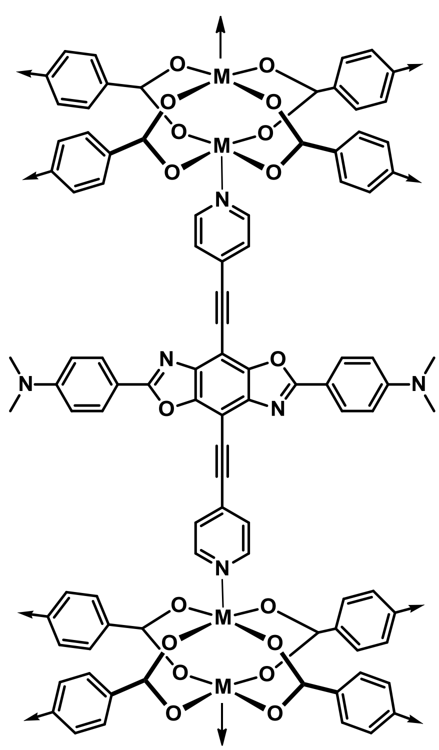

Figure 2.2 Predicted paddle-wheel carboxylate cluster pillared by cruciform **15**.

To pursue a goal to construct cruciform-MOFs substituted with electron-rich and acid-responsive dimethylaminophenyl moieties, paddle-wheel cluster with carboxylates in horizontal axis and bipyridyl cruciform pillar is proposed (the expected topology of cruciform **15**-MOF in Figure 2.2). Diverse combination of carboxylic and pyridyl ligands were tried and are shown in Figure 2.3. Dimethylformamide (DMF), diethylformamide (DEF), dimethylacetamide (DMA), dimethyl sulfoxide (DMSO), ethanol (EtOH), methanol (MeOH), water, and their mixtures were used as the solvents for the solvothermal synthesis. Although a great deal of crystalline-like materials have been produced from the combination of two ligands including dimethylaniline-substituted cruciforms thus far, notable single crystals have not yet been obtained to identify specific crystal structure using single crystal X-ray crystallography. Speculatively, such an inadequate result could be rationalized by preference of that cruciform precursor to rapidly precipitate rather than to mix with other components in the solvent to get the time to form the nucleus of crystal due to the low solubility in the majority of solvents.

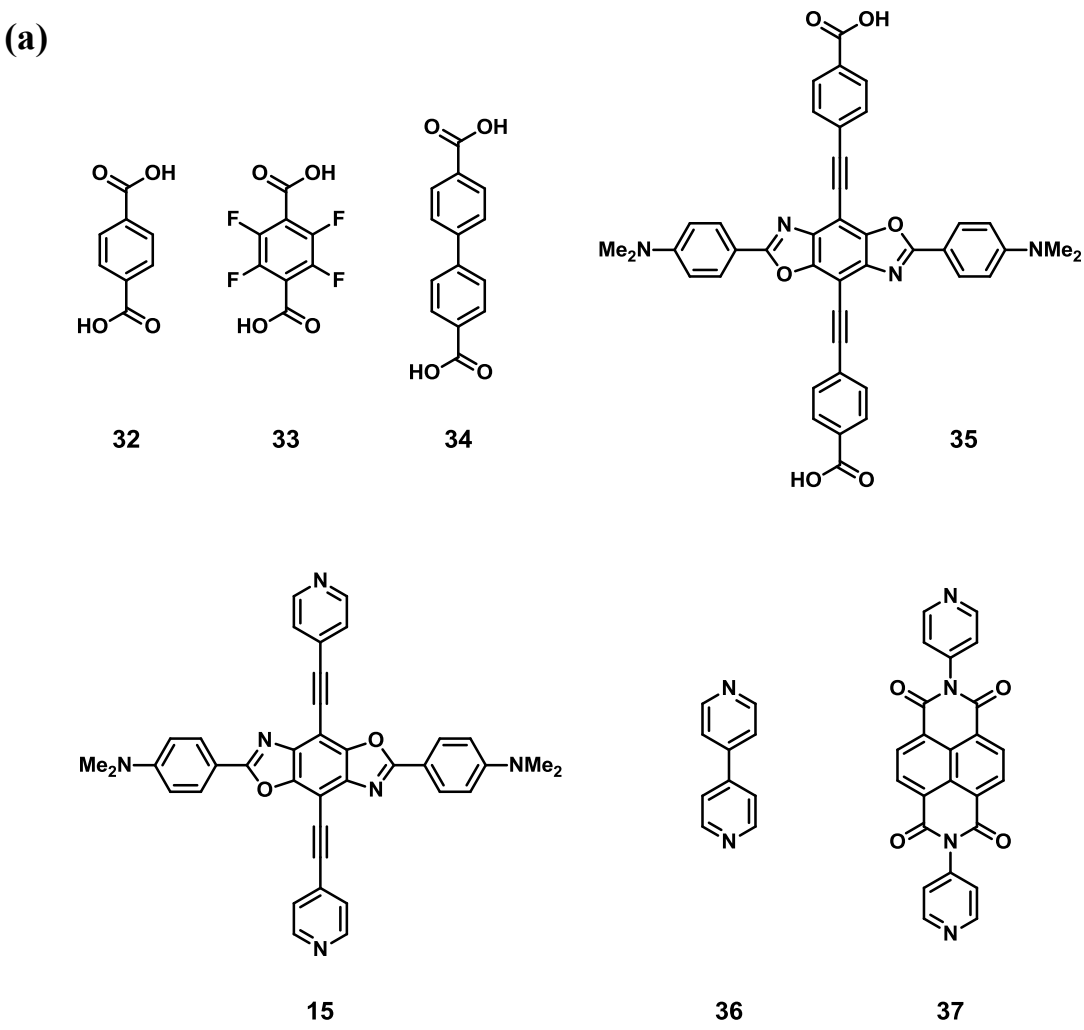

L	32	33	34	35	35	35
P	15	15	15	36	37	15

M = Zn, Cu, Co, Cd, etc.

Figure 2.3 (a) Library of organic linkers used in the synthesis of cruciform-containing MOFs; (b) intended paddle-wheel node with linkers (L) and pillars (P).

2.2.3 X-ray Crystal Structure Analysis of Cruciform-MOF 17

The single-crystal X-ray structure of cruciform-MOF **17** revealed a rectangular prismatic structure, which was classified as monoclinic crystal system with space group *I*2/a, (Table 2.1) and the asymmetric unit includes one zinc ion, one BDC ligand, and one cruciform **16** ligand (Figure 2.4). Each zinc(II) ion was coordinated with two oxygen atoms in one bidentate carboxyl group and other two oxygens from two monodentate

Table 2.1 Crystallographic data for **17**.

Compound name	**17**
Chemical formula	$C_{46}H_{40}N_4O_{10}Zn_6$
Formula Mass	1201.04
Crystal system	Monoclinic
a/Å	14.8997(13)
b/Å	35.889(3)
c/Å	19.6899(17)
α/°	90
β/°	106.085(2)
γ/°	90
Unit cell volume/Å ^{3}	10116.7(15)
Temperature/K	293(2)
Space group	*I*2/*a*
No. of formula units per unit cell, *Z*	8
Radiation type	Mo-Kα
Absorption coefficient, μ/mm^{-1}	2.856
No. of reflections measured	51984
No. of independent reflections	11596
R_{int}	0.1869
R_1 ($I > 2\sigma(I)$)	0.0860
$wR(F^2)$ ($I > 2\sigma(I)$)	0.2279
R_1 (all data)	0.1730
$wR(F^2)$ (all data)	0.2632
Goodness of fit on F^2	1.046

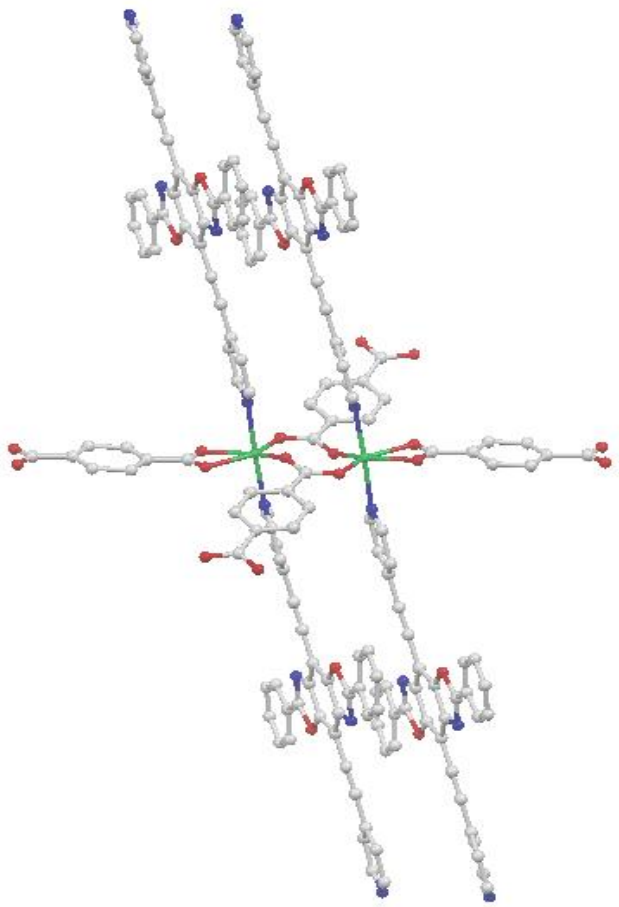

Figure 2.4 The coordination mode of the zinc ions in the crystal structure of **17**. Hydrogen atoms are omitted for clarity. The gray, red, blue, and green spheres represent the carbon, oxygen, nitrogen, and zinc atoms, respectively.

carboxyl groups of different BDC ligands. Axial positions of zinc carboxylate unit are occupied by two nitrogens from two different cruciform **16** linkers. As shown in Figure 2.4, two zinc(II) atoms are connected by two bridged COO^{-} moieties, and this dimeric complex is further linked to neighboring BDC ligands on both sides to form a 2D infinite sheet. The 2D sheets are pillared by cruciform **16** to complete a 3D framework, where

each two cruciforms alternated between two 2D sheets (Figure 2.5). A recent literature report discusses a Zn-based MOF—investigated as a heterogeneous asymmetric catalyst for aldol reaction—wherein a similar topology of inorganic subunit to ours was described.[60] In this structure, two types of organic ligands—dimethyl-5-(prop-2-ynyloxy)isophthalic acid and 4,4-dipyridine—were connected to the Zn center in the same asymmetric manner as our Zn cluster. However, Zn and carboxylic acid creates 1D chain while two chains are linked by dipyridne to cause 2D planes, which are stacked in a parallel fashion to form 1D channel.

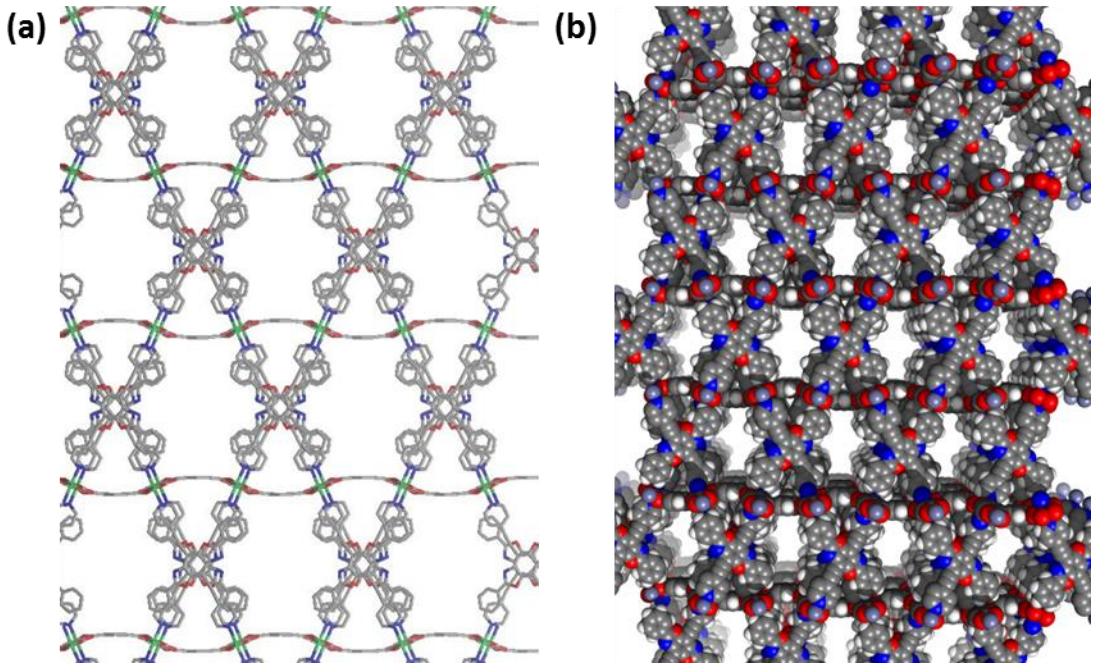

Figure 2.5 (a) Expanded crystal structure of **17**, (b) space-filling representations along the crystallographic *a* axis.

2.3 Conclusions and Outlook

In summary, two fully conjugated benzobisoxazole cruciform molecules (**15** and **16**) with pyridyl substitution along the precursor molecule's *y* axis have been synthesized. In particular, new synthetic method for cruciform **15** had been suggested through large-scale reaction in improved yield. Besides, the attempts of the incorporation of these prepared cruciforms into frameworks shows the potential for solid-state sensing system, where analytes could be transferred to the interior binding site on cruciforms through appropriately sized pores of frameworks. However, further experiments are needed to accomplish MOFs based on cruciform **15**, which exhibits good sensing ability in solution state. Additionally, the low solubility of cruciform **15** may be presenting a problem in crystallization of the derived MOFs, and that problem might be alleviated through either the synthesis of more soluble derivatives of **15**, or through the use of different cosolvent combinations in the crystallization process. In our future work, the incorporation of other cruciforms decorated with different end-groups into porous networks will also be attempted.

2.4 Experimental Section

2.4.1 General Procedures

All reagents and solvents were obtained from commercial suppliers and used without further purification. Solvents were used as received, except acetonitrile (MeCN), which was dried over activated alumina in an mBraun Solvent Purification System. Triethylamine (Et_3N) and diisopropylamine (*i*-Pr_2NH) were used after distillation over

KOH pellets and 20-minute degassing with nitrogen purge. Compound $PdCl_2(PPh_3)_2$[61] was prepared according to a published procedure. Microwave-assisted reaction was conducted in a Biotage Initiator 2.0 microwave reactor, producing monochromatic microwave radiation with the frequency of 2.45 GHz. Column chromatography was carried out on silica-gel 60, 32–63 mesh. Analytical TLC was performed on JT Baker plastic-backed silica gel plates. ^{1}H-NMR was recorded on JEOL ECX-400 and ECA-500 spectrometers, with working frequencies (for ^{1}H nuclei) of 400 and 500 MHz, respectively. ^{1}H NMR chemical shifts are reported in ppm units relative to the residual signal of the solvent ($CDCl_3$: 7.26 ppm, DMSO-d_6: 2.50 ppm), and multiplicity is expressed as follows: s = singlet, d = doublet, m = multiplet. All NMR spectra were recorded at 25 ℃. Single crystal X-ray diffraction measurements were performed at the Texas State University–San Marcos X-ray laboratory, using a Rigaku SCX-Mini diffractometer, equipped with a Mo tube and SHINE optics. Crystals were mounted on a glass fiber for measurement. Data collection and data integration were completed using Process-Auto. Solutions were generated by direct methods using SHELXS-97, and refined by full-matrix least squares on F^2 using SHELXL-97. All non-hydrogen atoms were refined anisotropically, and all aromatic hydrogen atoms were generated and refined using a riding model. SQUEEZE routine was used to treat the unknown disordered solvent contribution in the crystal and has been noted in the CIF file.

2.4.2 Synthesis of Bromanil

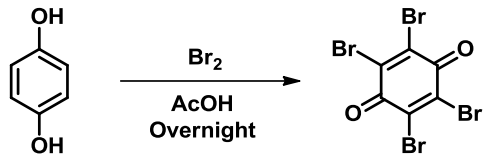

18 **19**

68 %

Hydroquinone (10.0 g, 90.8 mmol) was suspended in glacial acetic acid, and bromine (28.2 mL, 545 mmol) was added while stirring. After the mixture was allowed to stand overnight, some water and a small quantity of concentrated nitric acid were added, and the suspension was heated on the water bath for a short time to complete the bromination. It was then cooled down, and the precipitated bromanil was washed with water, dried, and recrystallized from glacial acetic acid to give 26.4 g (68%, 62.3 mmol) of the pure product. Spectral data agree with a previous literature report.[62]

2.4.3 Synthesis of 2,5-diamino-3,6-dibromoquinone

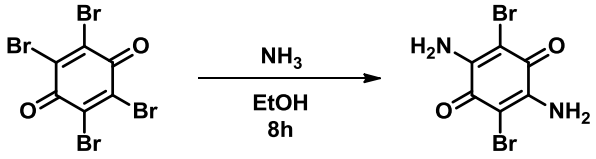

19 **20**

77 %

Bromanil (26.0 g, 61.4 mmol) was slurried into 300 mL of absolute Ethanol in a two-necked 500 mL round-bottomed flask fitted with a Friedrich's condenser connected to a balloon. While stirring, ammonia was added into the flask via a needle until the

balloon was full. The mixture was maintained at reflux for 8 h. The solution was then cooled, vacuum filtered, and washed with water, ethanol, and ether. The solid was air dried to give 14.0 g (77%, 47.4 mmol) of red powder. Due to its insolubility, this material was used without further purification. Spectral data agree with a previous literature report.[63]

2.4.4 Synthesis of 2,5-diamino-3,6-dibromohydroquinone

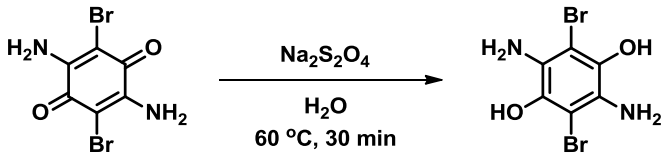

20 **21**

91 %

2,5-Diamino-3,6-dibromoquinone (2.00 g, 6.76 mmol) was mixed with $Na_2S_2O_4$ (3.32 g, 16.2 mmol) in 100 mL of water and stirred vigorously in the water bath at 60 ℃ until the red color of the starting material had disappeared. The mixture was filtered and washed with water, ethanol, and ether, and then air dried to give 1.84 g (91%, 6.17 mmol) of the desired product. The material was used without purification. Spectral data agree with a previous literature report.[63]

2.4.5 Synthesis of 2,6-diphenyl-4,8-dibromobenzo[1,2-*d*;4,5-*d′*]bisoxazole

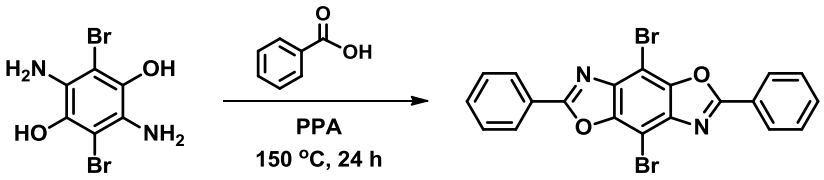

21 **22**

80 %

Compound **21** (2.86 g, 9.59 mmol) and benzoic acid (3.03 mg, 21.1 mmol) were mixed with polyphosphoric acid (20.0 g) in a 100 mL round-bottom flask equipped with a Friedrich's condenser. After heated at 150 ℃ for 24 h, the mixture was cooled, neutralized with aqueous 1M NaOH solution, and then filtered. The dark solid was washed with water, ethanol, and ether. The solid was air dried to give 3.60 g (80%, 7.66 mmol) of crude compound **22**. Due to its extremely low solubility, this material was used without further purification. Spectral data were consistent with literature reports.[9c]

2.4.6 Synthesis of 4-[2-(trimethylsilyl)ethynyl]pyridine

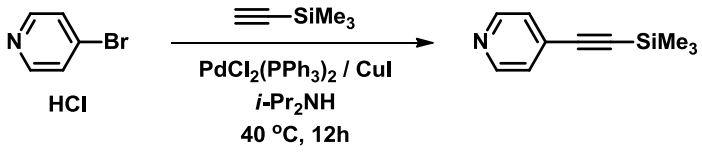

30 **31**

84%

4-Bromopyridine hydrochloride (500 mg, 2.57 mmol), $PdCl_2(PPh_3)_2$ (45.1 mg, 0.06 mmol), and CuI (12.2 mg, 0.06 mmol) were added in a round-bottom flask containing *i*-Pr_2NH (10mL). Trimethylsilylacetylene (0.70 mL, 5.14 mmol) was injected

to the mixture flask via a syringe while flushed with nitrogen. The reaction mixture was stirred at reflux for 12 h at 40 °C and quenched with water. The resultant suspension was extracted with CH_2Cl_2, and then the organic layer was dried over $MgSO_4$. After filtration, solvent was removed under reduced pressure. The crude solid was purified by column chromatography, eluting with hexane and ethyl acetate (90:10 ratio). The solvent was removed under reduced pressure to give the desired product in 84% yield (380 mg, 2.16 mmol). Spectral data were consistent with literature reports.[53b]

2.4.7 Synthesis of 4-ethynylpyridine

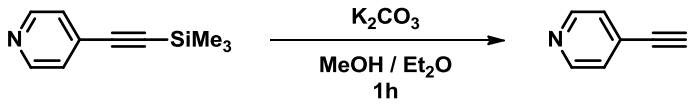

31 29

Anhydrous K_2CO_3 (3.01 g, 21.7 mmol) was added to a solution of 4-[2-(trimethylsilyl)ethynyl]pyridine (380 mg, 2.17 mmol) in a mixture of MeOH (10 mL) and Et_2O (10 mL). After stirring for 1 h, the reaction mixture was quenched with 1 mL of water and concentrated under reduced pressure. The solid was dissolved in CH_2Cl_2 and filtered through celite. The solvent was removed under reduced pressure to give crude 4-ethynylpyridine and used quickly without further purification due to sensitivity issue. Spectral data were consistent with literature reports.[53a]

2.4.8 Synthesis of Cruciform 16

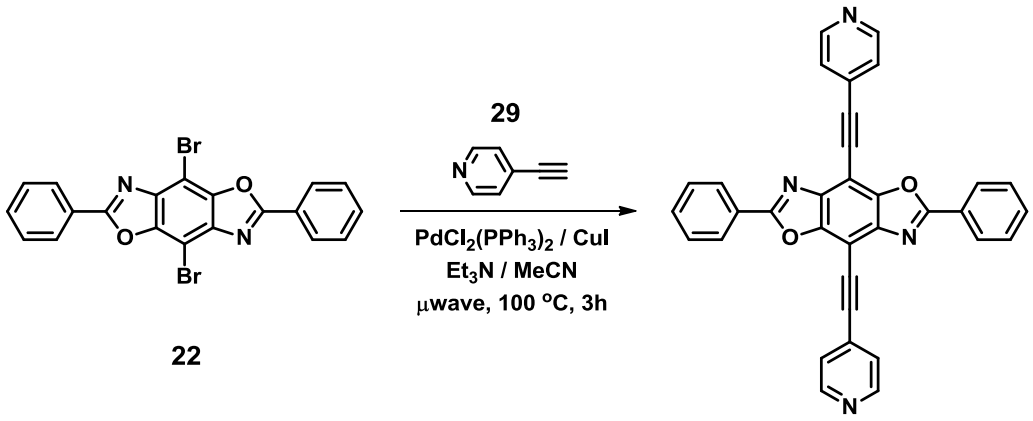

2,6-Diphenyl-4,8-dibromobenzo[1,2-*d*;4,5-*d′*]bisoxazole (compound **22**, 430 mg, 0.91 mmol), $PdCl_2(PPh_3)_2$ (96.4 mg, 0.13 mmol), and CuI (10.5 mg, 0.06 mmol) were added to a thick-walled microwave pressure vial containing a degassed mixture of Et_3N (5 mL) and MeCN (5 mL). The entire amount of 4-ethynylpyridine, prepared above, was suspended in a small amount of degassed solvents and added to the mixture vial using a syringe under a flow of nitrogen gas. The vial was sealed and exposed to microwave irradiation for 3 h at 100 ℃. After cooling, the suspension was filtered with hexane, and the solid was further purified by column chromatography, eluting first with pure CH_2Cl_2, and then successively with CH_2Cl_2/MeOH mixtures in 97:3 and 95:5 ratios. The solvent was removed under reduced pressure to give yellow powder in 31% yield (146 mg, 0.28 mmol). Spectral data were consistent with literature reports.[9c] ^{1}H NMR ($CDCl_3$, 400 MHz): δ 8.74 (d, 4H), 8.42 (d, 4H), 7.65 (d, 4H), 7.60 (m, 6H) ppm.

2.4.9 Synthesis of 2,6-bis[*p*-(*N*,*N*-dimethylamino)phenyl]-4,8-dibromobenzo[1,2-*d*;4,5-*d′*]bisoxazole

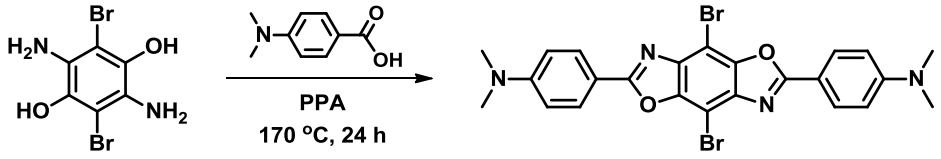

21 **23**

65 %

Compound **21** (899 mg, 3.02 mmol), 4-(*N*,*N*-dimethylamino)benzoic acid (1.10 g, 6.64 mmol) were mixed with polyphosphoric acid (14.0 g) in a 100 mL round-bottom flask equipped with a Friedrich's condenser. The mixture was stirred for 24 h while heating to 170 ℃. After cooling, the mixture was neutralized with aqueous 1M NaOH solution and filtered. The dark green solid was washed with water, ethanol, and then ether followed by air-drying. The crude solid was dissolved in CH_2Cl_2 and passed through a short silica gel column. The solvent was removed in vacuo to give 1.57 g (93%, 2.82 mmol) of the desired product **23**. Spectral data were consistent with literature reports.[9c]

2.4.10 Synthesis of Compound 26

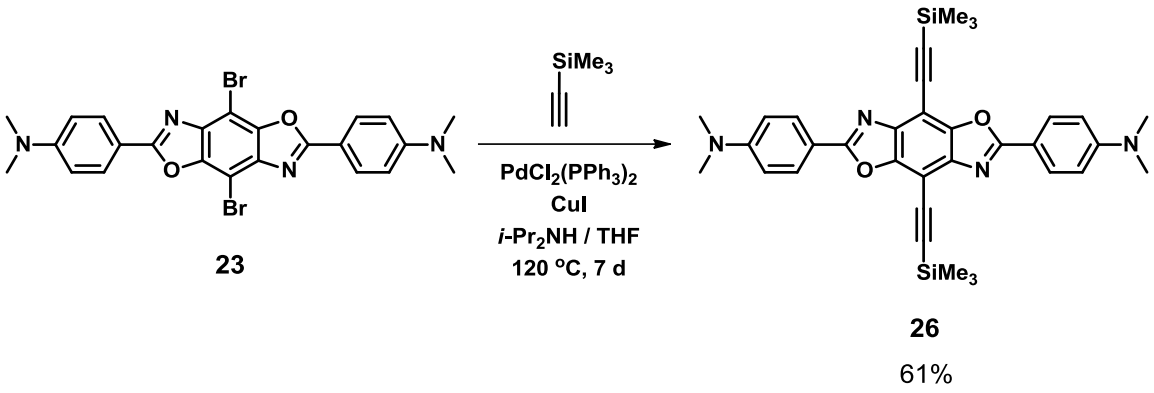

Using a syringe, degassed *i*-Pr_2NH (50 mL) and THF (50 mL) were added to a thick-walled pressure vessel containing 2,6-bis[*p*-(*N*,*N*-dimethylamino)phenyl]-4,8-dibromobenzo[1,2-*d*;4,5-*d*']bisoxazole (2.25 g, 4.04 mmol), $PdCl_2(PPh_3)_2$ (264 mg, 0.37 mmol), and CuI (35.8 mg, 0.18 mmol) under the flow of nitrogen gas. The resulting suspension was sonicated for 1 min, and then trimethylsilylacetylene (10.0 mL, 73.7 mmol) was added under nitrogen atmosphere. The vessel was sealed firmly, and the mixture was stirred and heated for 7 d at 120 °C. After cooling, the resultant mixture was evaporated under reduced pressure, and the residue was purified by silica gel column chromatography, eluting first with CH_2Cl_2/hexane mixtures (67:33, followed by 75:25), and then with pure CH_2Cl_2. The solvent was removed under reduced pressure to afford 1.45 g (61%, 2.45 mmol) of the desired compound **26** as a yellow powder (mp >350 °C, with decomposition). UV-Vis (THF): λ_{max} (log ε) = 440 (4.94), 350 (4.56), 333 (4.65), 319 (4.82) nm. IR (neat): 2957 (w, $\tilde{\nu}_{C-H}$), 2156 (w, $\tilde{\nu}_{C\equiv C}$), 1608 (s), 1585 (w), 1508 (s), 1436 (w), 1369 (w), 1333 (m), 1207 (w), 1250 (w), 1189 (m), 1171 (w), 1072 (w), 1013 (w), 1003 (w), 980 (m), 946 (w), 910 (m), 844 (s), 815 (m), 758 (w), 741 (w), 696 (w)

cm^{-1}. ^{1}H NMR ($CDCl_3$, 500 MHz): δ 8.20 (d, $^{3}J_{H-H}$ = 9.16 Hz, 4H), 6.78 (d, $^{3}J_{H-H}$ = 9.16 Hz, 4H), 3.09 (s, 12H), 0.40 (s, 18H) ppm. ^{13}C NMR ($CDCl_3$, 125 MHz): δ 165.4, 152.6, 149.1, 140.7, 129.7, 113.7, 111.5, 105.9, 97.2, 95.0, 40.2, 0.2 ppm. LRMS (ESI/[M + H]$^{+}$) calcd for $C_{34}H_{38}N_4O_2Si_2$ 591.25, found 591.42. Anal. Calcd for $C_{34}H_{38}N_4O_2Si_2 \cdot 1/4\ CH_2Cl_2$: C, 67.21; H, 6.34; N, 9.15. Found: C, 67.86; H, 6.40; N, 8.98.

2.4.11 Synthesis of Cruciform 15

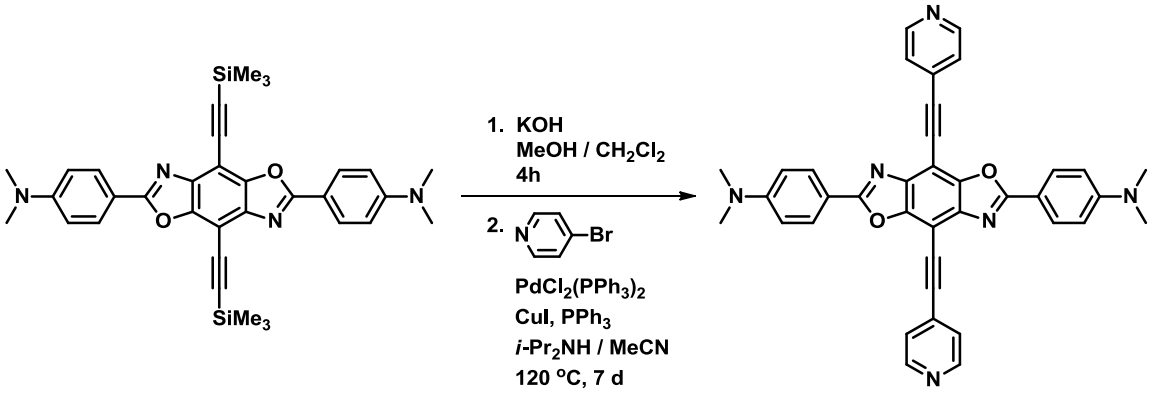

26 **15**

72%

KOH (588 mg, 9.21 mmol) was dissolved in MeOH (25 mL) and added to a solution of compound **26** (1.36 g, 2.30 mmol) in CH_2Cl_2 (50 mL). After stirring for 4 h, the resulting mixture was concentrated under reduced pressure. The solid was dissolved in chloroform, and then passed through a short silica gel column. The solvent was removed under reduced pressure giving desilylated compound in 63% yield (656 mg, 1.47 mmol).

Using a syringe, degassed *i*-Pr_2NH (25 mL) and MeCN (25 mL) were added to a thick-walled pressure vessel containing desilylated compound (656 mg, 1.47 mmol), 4-bromopyridine hydrochloride (1.16 g, 5.88 mmol), $PdCl_2(PPh_3)_2$ (42.1 mg, 0.06 mmol), CuI (5.7 mg, 0.03 mmol), and PPh_3 (15.7 mg, 0.06 mmol) under nitrogen atmosphere followed by the sonication for 1 min. The vessel was sealed firmly, and the mixture was stirred while heating for 7 d at 120 ℃. After cooling, the crude solid was washed with ethyl acetate, ethanol, and water, and then air dried to afford 637 mg (72%, 1.06 mmol) of the desired cruciform **15** as a red powder. Spectral data were consistent with literature reports.[9c] ^{1}H NMR ($CDCl_3$, 500 MHz): δ 8.70 (d, $^3J_{H–H}$ = 5.73 Hz, 4H), 8.23 (d, $^3J_{H–H}$ = 9.16 Hz, 4H), 7.64 (d, $^3J_{H–H}$ = 5.73 Hz, 4H), 6.80 (d, $^3J_{H–H}$ = 9.16 Hz, 4H), 3.11 (s, 12H) ppm.

2.4.12 Synthesis of Cruciform-MOF (17)

Cruciform **16** (20 mg, 0.039 mmol) and terephthalic acid (BDC, 12.9 mg, 0.078 mmol) were mixed in *N*,*N*′-dimethylformamide (DMF, 20 mL) and distributed equally to ten 8 mL vials. The solution of $Zn(NO)_3{\cdot}6H_2O$ (23.1 mg, 0.078 mmol) in ethanol (10 mL) was added evenly to ten vials. The vials were sealed with Teflon tape, capped firmly, and then heated in the oven at 80 ^{o}C for 3 days. The vials were removed and cooled to room temperature. The solvent was removed, and resulting crystalline materials were washed several times with fresh DMF. Most vials produced yellow rod-shaped crystals, which were characterized with single crystal X-ray crystallography. A portion of the solids was

digested with DMSO/DCl for ^{1}H NMR measurements. (DMSO, 500 MHz): δ 9.00 (d, 4H; **16**), 8.37 (d, 4H; **16**), 8.26 (d, 4H; **16**), 8.03 (s, 6H; BDC), 7.74 (m, 6H; **16**) ppm.

2.4.13 Single X-ray crystallographic data

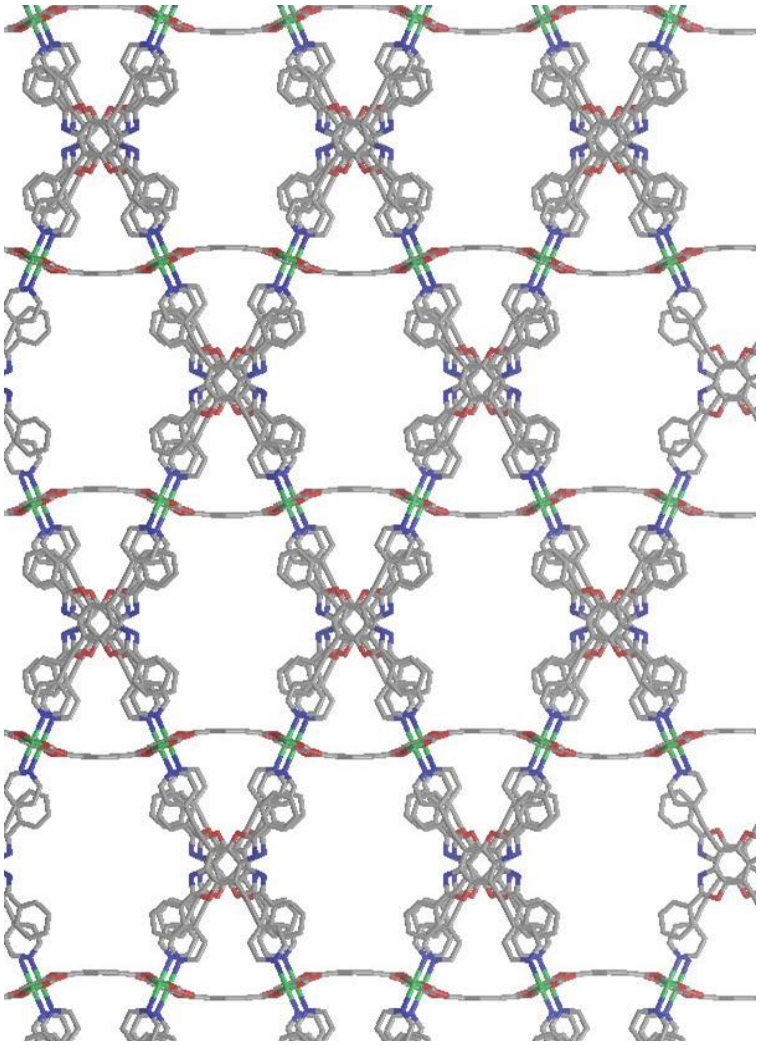

Figure 2.6 3D network of **17** along *a* axis. The gray, red, blue, and green colors represent the carbon, oxygen, nitrogen, and zinc atoms, respectively.

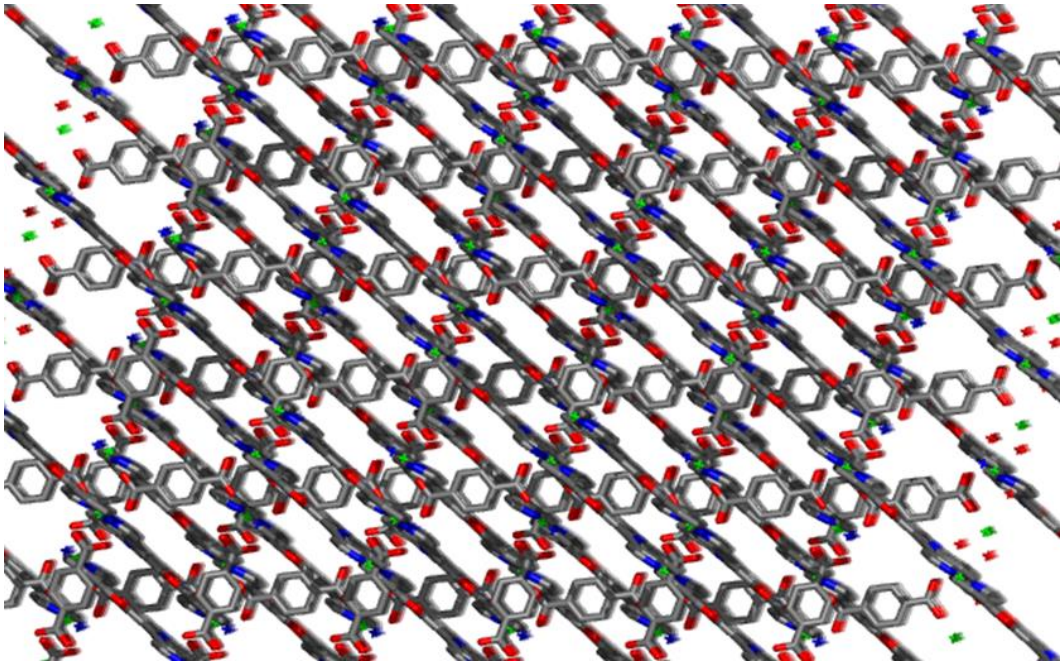

Figure 2.7 3D network of **17** along *b* axis.

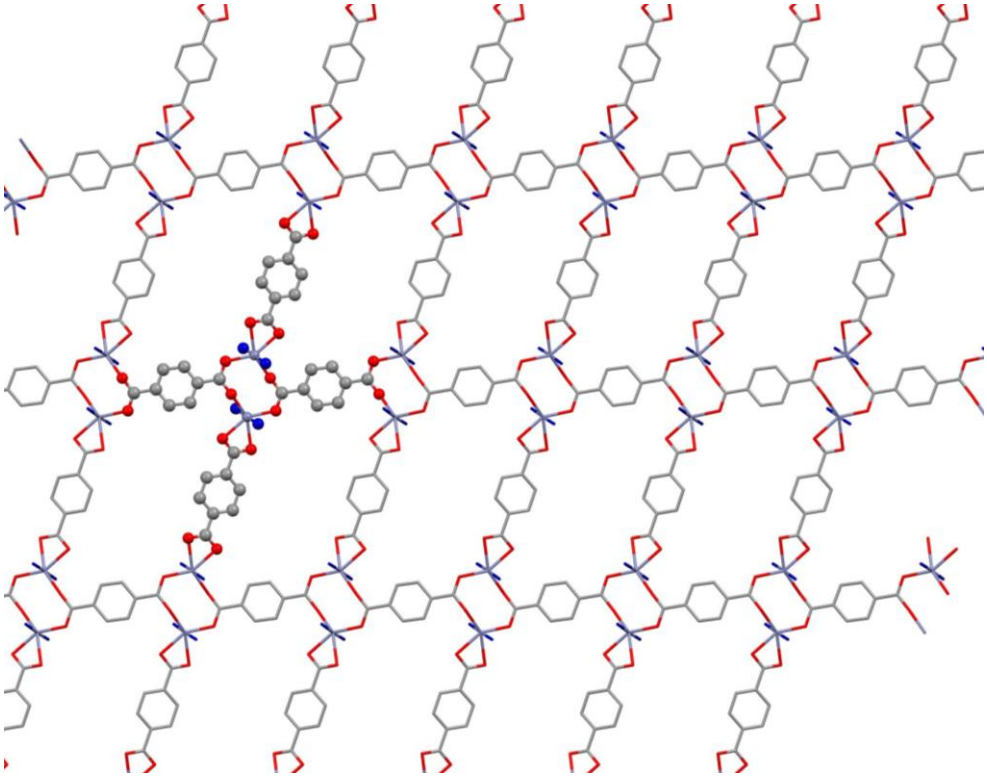

Figure 2.8 *ac* plane with omission of cruciform pillars.

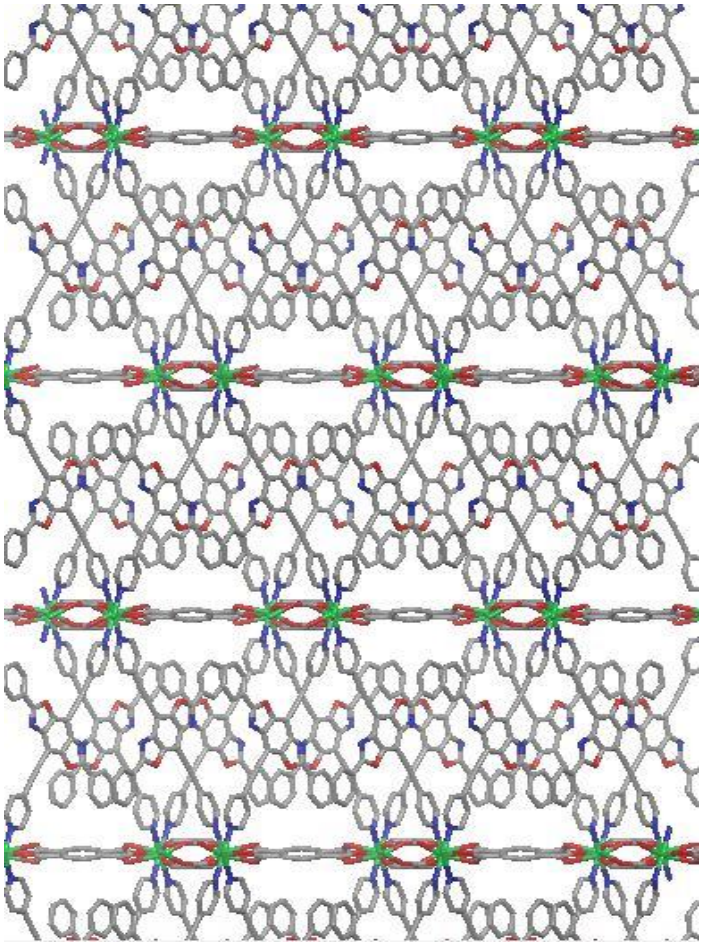

Figure 2.9 3D network of **17** along the crystallographic *c* axis.

2.4.14 Microscopy image of single crystal

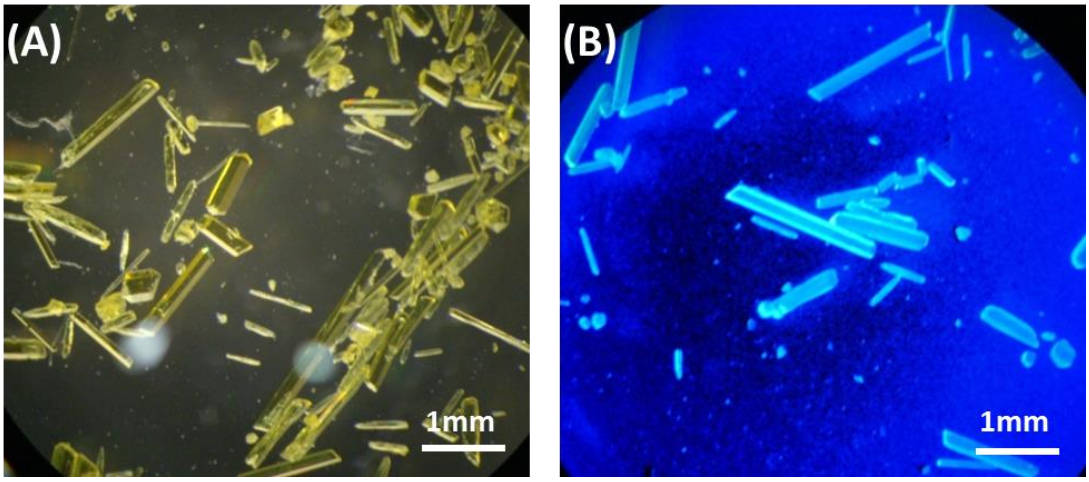

Figure 2.10 (A) Microscopy image of single crystal **17** revealing rod morphology. (B) crystal of **17** under the UV light (λ_{exc} = 365 nm).

Chapter Three

Selective and Sensitive Fluoride Detection through Alkyne Cruciform Desilylation

3.1 Introduction

During the past decade, cross-conjugated cruciform fluorophores[16s, 64] have been explored as versatile sensors for Brønsted and Lewis acids,[9c, 15b, 15g, 16b, 16s, 17b] metals,[16f, 16o] anions,[16a, 17a, 65] amines,[16g, 16j, 65-66] phenols,[17b] and other analytes. The great majority of these sensing protocols were reversible in nature, based on either coordinative or dynamically covalent interactions. While reversibility generally presents a desirable feature in sensor design, low association constants between the cruciforms and their analytes can limit the sensitivity of analyte detection. Conversely, operation of an irreversible and high-yielding covalent reaction on a cruciform sensor constitutes a pathway for highly sensitive detection, as an analyte needs to be added only in close-to-stoichiometric amount relative to the highly dilute fluorescent sensor. In this chapter, we illustrate this principle through the first use of benzobisoxazole cruciforms[9c, 17-18, 19b, 64] as irreversible, specific, and sensitive sensors for fluoride. Fluorine and silicon form a very strong bond (135 kcal mol^{-1}),[67] and thus fluoride-induced desilylation reactions proceed rapidly and irreversibly.[68] Sensing of fluoride ions through the cleavage of O–Si bonds (and the exploration of reactivity of the resultant O–H groups) was achieved by Kim and Swager,[69] and subsequently used by other groups—including in the context of physiologically relevant[70] sensing of fluoride in aqueous solutions. We speculated that fluoride could also be sensed by cleaving the C–Si bond in silylated alkynes, and that the

resultant change in the electronics of the triple bond would be readily transmitted through the conjugated circuit.

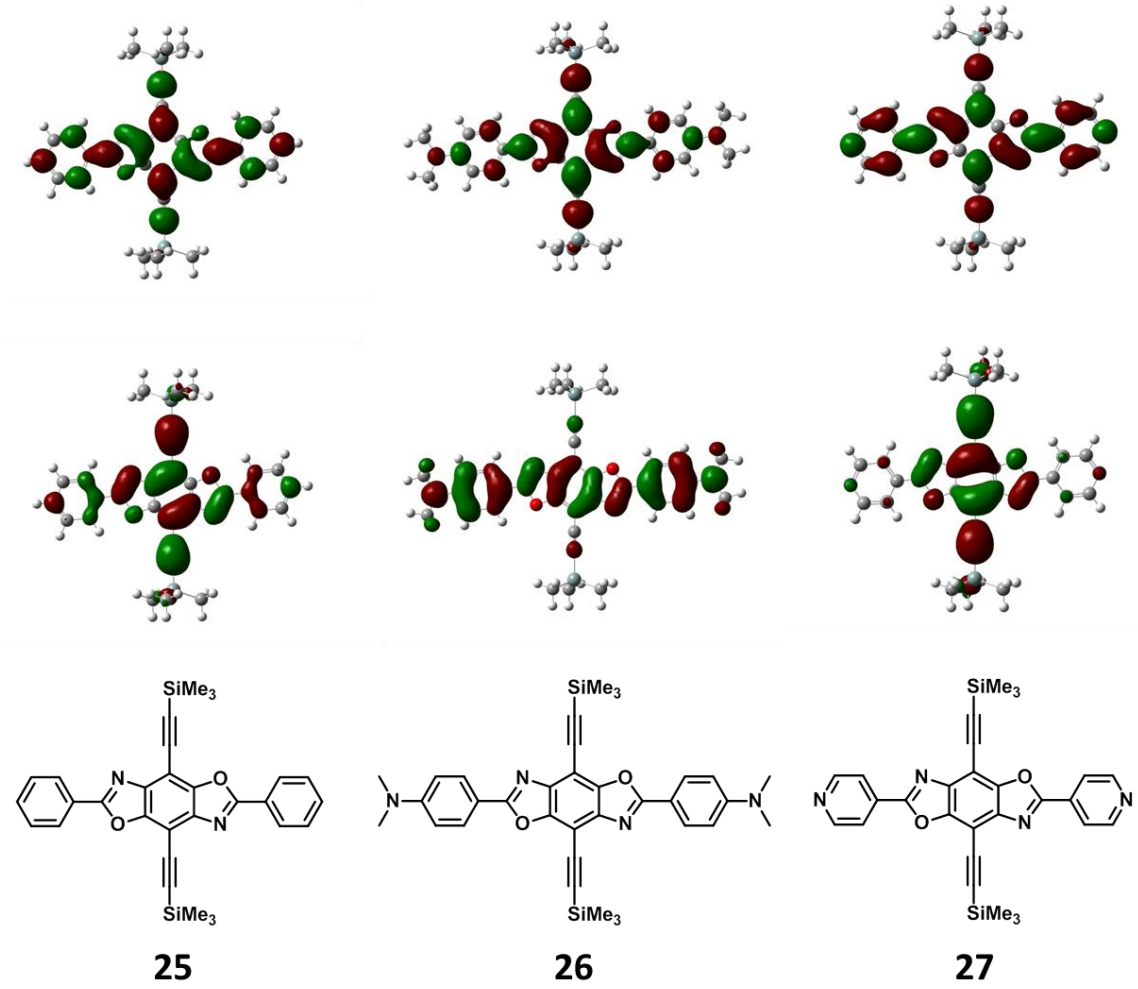

Figure 3.1 Frontier molecular orbitals (FMOs) of silylated cruciforms **25**–**27**. LUMOs are shown on first row, and HOMOs are below them. Spatial separation of FMOs is most pronounced in compound **27**.

3.2 Results and Discussion

3.2.1 Computational Studies

In order to assess the potential of silylated benzobisoxazole cruciforms as fluoride sensors, we first computationally evaluated the frontier molecular orbitals (FMOs) of three trimethylsilyl (TMS)-substituted compounds **25**–**27** (Figure 3.1) using Gaussian 09W software package at the B3LYP/3-21G level of theory. Graphical representations of highest occupied (HOMOs) and lowest unoccupied molecular orbitals (LUMOs) of **25**–**27** are shown in Figure 3.1. In phenyl-substituted cruciform **25**, FMOs are largely overlapping, suggesting that desilylation should have a similar effect on both orbitals—and thus lead to just a small change in the HOMO–LUMO gap. Similar situation is observed in cruciform **26** as well; in its case, the two FMOs were mostly positioned along the horizontal benzobisoxazole axis, but were still largely overlapping. However, in the pyridyl-based compound **27**, spatial separation of FMOs is noticeable: HOMO is positioned along the electron-richer vertical axis, while the LUMO chiefly resides along the pyridine-bearing horizontal axis. This orbital distribution suggested that the desilylation of **27** should impact HOMO and LUMO unevenly and thus constitute the basis of an optical response of cruciform **27** to fluoride addition.

3.2.2 Synthesis of Materials

Encouraged by this computational insight, we synthesized TMS-substituted cruciforms **25**–**27**, as well as compound **28**—the triisopropylsilyl (TIPS)-substituted analog of **27** (Scheme 3.1). All four silylated cruciforms were expected to desilylate

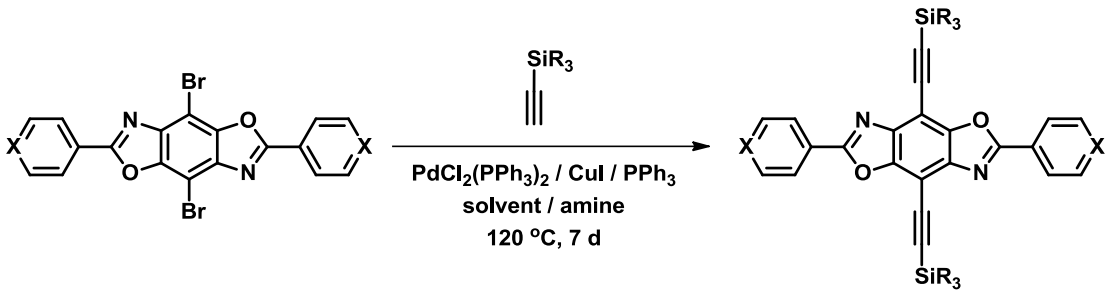

22 X = CH
23 X = C–NMe_2
24 X = N

25 X = CH R = Me 42%
26 X = C–NMe_2 R = Me 61%
27 X = N R = Me 44%
28 X = N R = *i*-Pr 54%

Scheme 3.1 Synthesis of fluorophores **25**–**28**.

under the influence of fluoride, but cruciform **28** was the only one that was expected to be desilylated exclusively with fluoride—compounds **25**–**27** could also be deprotected by hydroxide or other basic species.[71] Starting with brominated benzobisoxazoles **22**–**24** (Scheme 3.1),[9c] Sonogashira coupling with TMSacetylene produced corresponding silylated compounds **25**–**27** in moderate yields. Triisopropylsilyl-substituted cruciform **28** was prepared in 54% yield by reacting **24** with TIPSacetylene. Compounds **25**–**28** are yellow to dark orange powders, with strong fluorescence in solution.

3.2.3 Optical Response to Anions

Optical response of silylated benzobisoxazoles to anions was evaluated by UV/Vis absorption and fluorescence spectroscopy. Dilute solutions (10^{-5} M for absorption and 10^{-7} M for fluorescence measurements) of **25**–**28** in THF were titrated with concentrated solutions (10^{-2} to 10^{-4} M) of tetrabutylammonium fluoride, chloride,

bromide, iodide, hydroxide, acetate, phosphate, and nitrate. In Figure 3.2, fluorescence titration spectra for addition of fluoride are shown. The absorption titration spectra for fluoride and all (absorption and fluorescence) spectra for the titration of **25**–**28** with other anions are given in the experimental section.

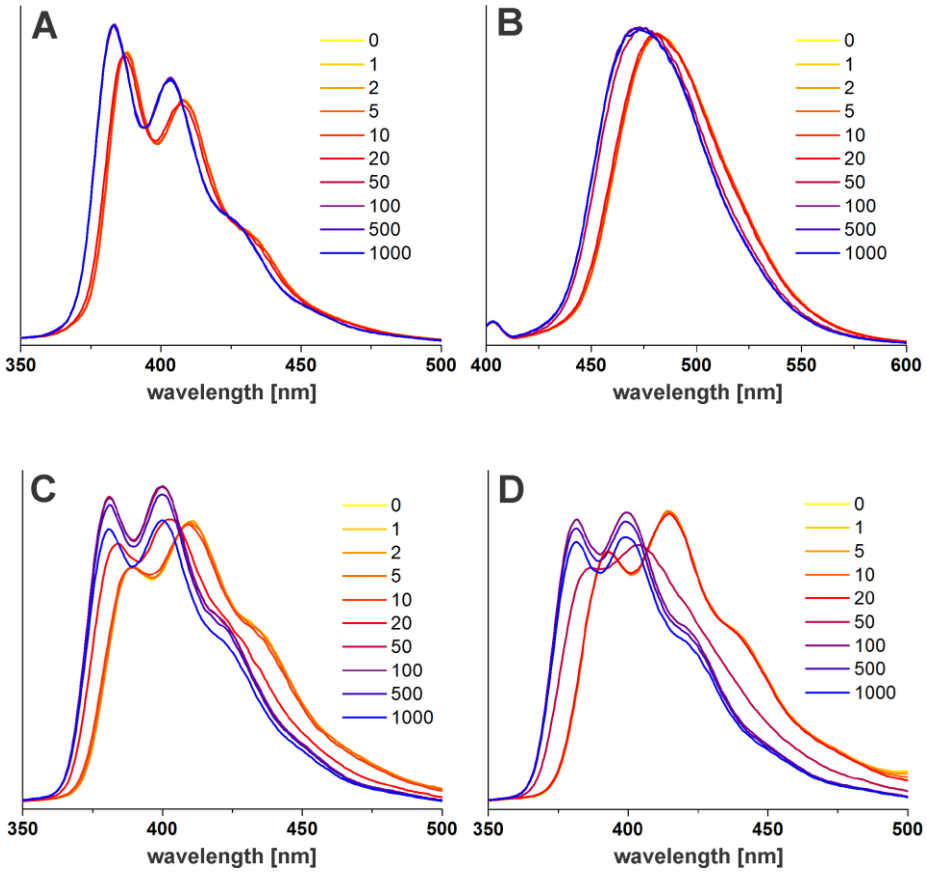

Figure 3.2 Normalized fluorescence intensity plots for the titrations of 10^{-7} M THF solutions of **25** (A), **26** (B), **27** (C), and **28** (D) with a 10^{-4}–10^{-2} M solution of $TBA^+ F^-$. Excitation wavelengths were: 303 nm for **25**, 360 nm for **26**, and 306 nm for **27** and **28**. Numbers on the right side of each graph represent the number of equivalents of $TBA^+ F^-$ added.

Following the addition of fluoride, the fluorescence emission maxima of all four fluorophores underwent a blue shift. This behavior is consistent with the broadening of the HOMO–LUMO gap, which in turn is explained by the dominant stabilization of the HOMO upon desilylation.[72] The emission of compound **25** shifted by approx. −5 nm upon exposure to ~100 equiv. of fluoride and those changes are very similar to those observed upon the addition of hydroxide anion. Small changes in absorption and fluorescence can be rationalized through the relatively similar spatial distribution of FMOs of **25**, while the nonspecific response comes from the easy cleavage of the TMS group, which can be deprotected using either hydroxide or fluoride anions. Similarly, compound **26** showed noticeable but relatively small shifts in absorption and fluorescence spectra—and these shifts were induced by fluoride and hydroxide alike.

Cruciforms **27** and **28** exhibited the most diagnostic shifts in absorption (as shown in the experimental section) and especially fluorescence upon addition of fluoride, with emission maxima shifting by −15 nm in the case of **28**. After the addition of an excess of fluoride (>50 equiv.), the fluorescence profiles of **27** and **28** appeared largely identical—which is logical, as both compounds desilylate to the same terminal diyne.

The crucial difference between **27** and **28** resided in the lability of their silyl groups. Thus, the trimethylsilyl group of **27** can be cleaved with fluoride, but also with hydroxide, acetate, and phosphate, as evidenced by their similar fluorescence titration profiles proven in the following experimental section. On the other hand, the more stable TIPS protecting group is cleaved only with fluoride (on the timescale of our experiments) and thus only fluoride induces the noteworthy shifts in the fluorescence spectrum shown

in Figure 3.2 (D). In order to quantify the selectivity of fluoride detection with **28**, we plotted the relative changes in the intensity of its fluorescence emission at 381 nm, following the addition of 100 equiv. of different anions (Figure 3.3). Fluoride addition

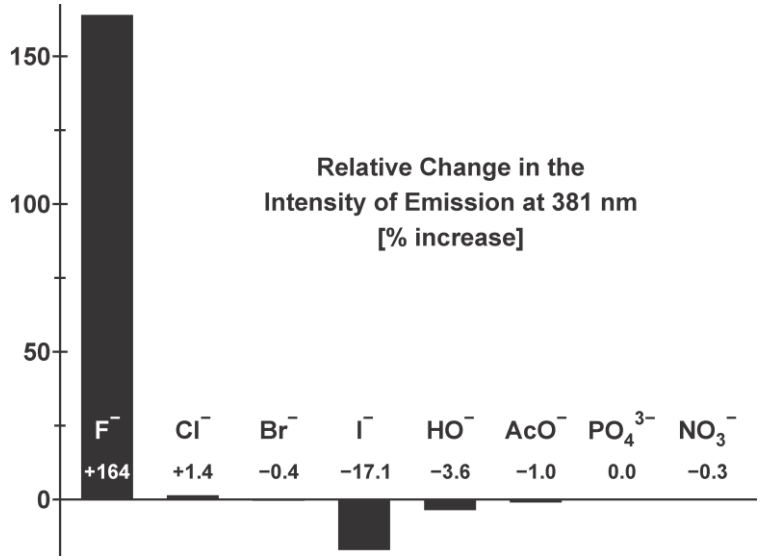

Figure 3.3 Relative changes in the intensity of emission of **28** at 381 nm upon addition of 100 equiv. of corresponding analytes. Excitation wavelength was 306 nm, and the percentage values were calculated as $\%_{increase} = (I_{100}–I_0)/I_0$, where I_{100} and I_0 are intensities of fluorescence with 100 and 0 equiv. of analyte, respectively.

enhances the emission of **28** at 381 nm by more than 1.5 times; in contrast, chloride, bromide, hydroxide, acetate, nitrate, and phosphate all changed the emission of **28** at this wavelength by less than 4%. Iodide anion somewhat quenched the fluorescence of **28** (−17.1%), which can be rationalized through heavy atom-induced collisional quenching, but without significant shifts in the position of emission maxima. This behavior did not interfere with fluoride detection, as it required ~1000 equiv. of iodide to decrease

fluorescence intensity by approx. 70%. The fluorescence emission changes that accompany the addition of fluoride and other anions are visible by naked eye for sensors **27** and **28** (Figure 3.4). The switch of the emission color from cyan to purple is clearly observable for fluoride and hydroxide in the case of **27**, and only for fluoride when cruciform **28** is used.

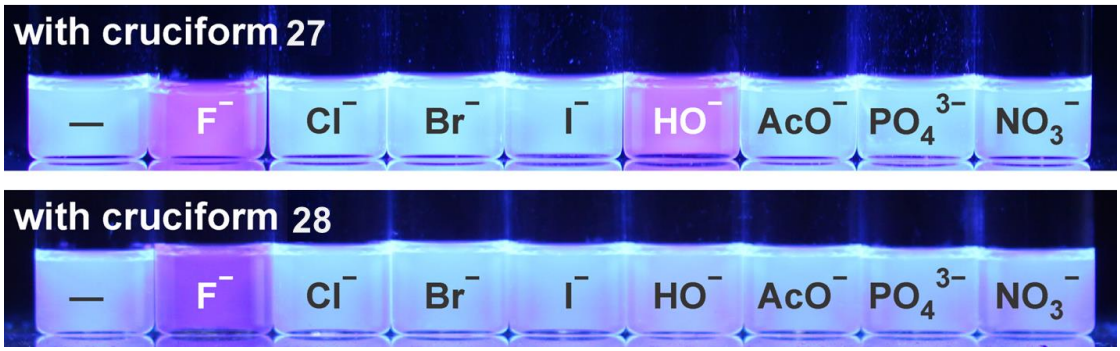

Figure 3.4 Changes in emission colors of dilute solutions of cruciforms **27** (top) and **28** (bottom) upon addition of 10 equiv. of the corresponding anions. Excitation wavelength was 365 nm.

3.3 Conclusions and Outlook

In conclusion, this study has shown that silylated benzobisoxazole cruciforms can serve as selective and sensitive fluorescent detectors for fluoride anion. Their emission changes in response to fluoride addition; these changes are spectroscopically observable at fluoride concentrations as low as 50 μM and are highly specific for this anion. They operate through the desilylation of silylated alkynes, and are thus rare among other

desilylation-based fluoride sensors which are primarily exploring the cleavage of the Si–O bond. More generally, we believe that this work demonstrates that versatility of the "cruciform approach" to sensing. As benzobisoxazole and other conjugated cruciforms can be very easily induced to spatially isolate their FMOs, creation of a viable sensor is highly predictable. Synthetic attention can instead be focused on the relatively small modifications that can change sensor specificity and selectivity dramatically, allowing expedient adaptation of a cruciform sensor to a wide variety of analytes. This strategy is perhaps best illustrated in the current work, where silylated alkyne cruciforms—which are in fact common synthetic precursors to more complex alkynes—can be used as selective sensors of their own desilylation.

3.4 Experimental Section

3.4.1 General Methods

All reagents were purchased from commercial suppliers and used without further purification. Solvents were used as received, except tetrahydrofuran (THF), which was dried over activated alumina in an mBraun solvent Purification System. Triethylamine (Et_3N) and diisopropylamine (*i*-Pr_2NH) were distilled over KOH pellets. All solvents were degassed by a 20 min nitrogen purge prior to use. Compounds $PdCl_2(PPh_3)_2$[61] and dibromobenzobisoxazole compounds (**22**, **24**)[9c] were prepared according to literature procedures. Synthesis of cruciform **26** is described in chapter 2. THF (AR grade) was used to perform analytical studies. All the UV-Vis spectra were recorded on a Perkin-Elmer Lamda 25 UV/Vis spectrophotometer. All the fluorescence spectra were recorded

on a Perkin-Elmer Fluorescence Analyzer LS-45 spectrofluorometer. ^{1}H NMR spectra were obtained on JEOL ECX-400 and ECA-500 spectrometers, with working frequencies of 400 and 500 MHz, respectively. All ^{13}C NMR spectra were recorded with simultaneous decoupling of ^{1}H nuclei. ^{1}H NMR chemical shifts are reported in ppm units relative to the residual signal of the solvent ($CDCl_3$: 7.26 ppm), and multiplicity is expressed as follows: s = singlet, d = doublet, m = multiplet. All NMR spectra were recorded at 25 °C. Mass spectral measurements were performed by the Mass Spectrometry Facility of the Department of Chemistry at the University of Houston. Infrared spectra were recorded on a Perkin-Elmer Spectrum 100 FT-IR spectrophotometer using Pike MIRacle Micrometer pressure clamp. Microanalyses were conducted by Intertek USA, Inc. Melting points were measured in open capillary tubes using Mel-Temp Thermo Scientific apparatus and are uncorrected. Column chromatography was carried out on silica gel 60, 32–63 mesh. Analytical TLC was performed on JT Baker plastic-backed silica gel plates.

3.4.2 Synthesis of Cruciform 25

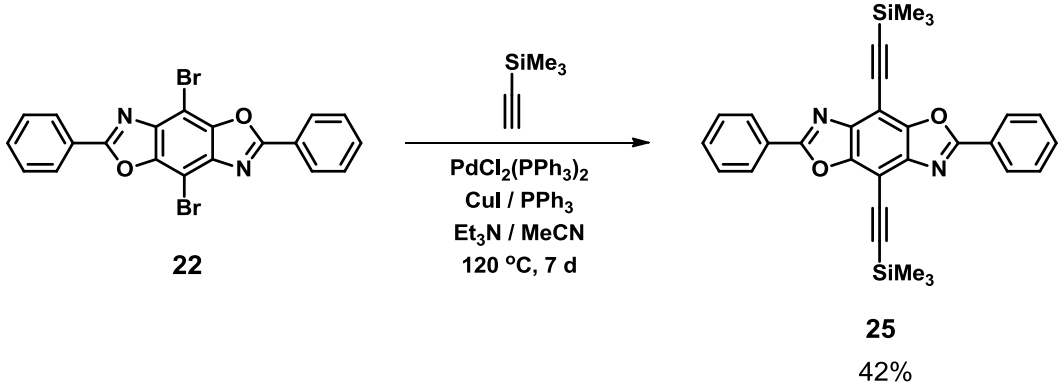

Using a syringe, degassed Et_3N (20 mL) and MeCN (20 mL) were added to a thick-walled pressure vessel containing 2,6-diphenyl-4,8-dibromobenzo[1,2-*d*;4,5-*d'*]bisoxazole (1.00 g, 2.13 mmol), $PdCl_2(PPh_3)_2$ (59.7 mg, 0.085 mmol), CuI (8.1 mg, 0.043 mmol), and PPh_3 (22.3 mg, 0.085 mmol) under nitrogen. This suspension was sonicated for 1 min, and then trimethylsilylacetylene (3.06 mL, 21.3 mmol) was added under nitrogen atmosphere. The vessel was sealed firmly, and the mixture was stirred and heated for 7 d at 120 ^oC. After cooling, the resultant mixture was evaporated under reduced pressure, and the residue was purified by silica gel column chromatography, eluting first with hexane/ethyl acetate mixtures (from 90:10 to 80:20), and then with pure CH_2Cl_2. After evaporation of solvent, the desired compound **25** was isolated as a light yellow powder in 42% yield (466 mg, 0.884 mmol) with mp of 317 ºC. UV-Vis (THF): λ_{max} (log ε) = 379 (4.83), 360 (4.80), 291 (4.88), 280 (4.63) nm. IR (neat): 2961 (w, $\tilde{\nu}_{C-H}$), 2155 (w, $\tilde{\nu}_{C\equiv C}$), 1609 (w), 1587 (w), 1561 (w), 1561 (w), 1488 (w), 1450 (w), 1337 (m), 1265 (w), 1251 (w), 1079 (w), 1064 (w), 1028 (w), 1010 (w), 982 (w), 920 (w), 851 (s), 759 (w), 723 (w), 697 (m), 685 (m) cm^{-1}. ^1H NMR ($CDCl_3$, 400 MHz): δ 8.37 (m, 4H), 7.57 (m, 6H), 0.42 (m, 18H) ppm. ^{13}C NMR ($CDCl_3$, 100 MHz): δ 164.6, 149.3, 141.1, 132.1, 129.0, 128.2, 126.6, 107.3, 98.7, 94.2, 0.1 ppm. LRMS (ESI/$[M + H]^+$) calcd for $C_{30}H_{28}N_2O_2Si_2$ 505.17, found 505.16. Anal. Calcd for $C_{30}H_{28}N_2O_2Si_2 \cdot 1/4\ CH_2Cl_2$: C, 69.08; H, 5.46; N, 5.33. Found: C, 69.15; H, 5.37; N, 5.26.

3.4.3 Synthesis of Cruciform 27

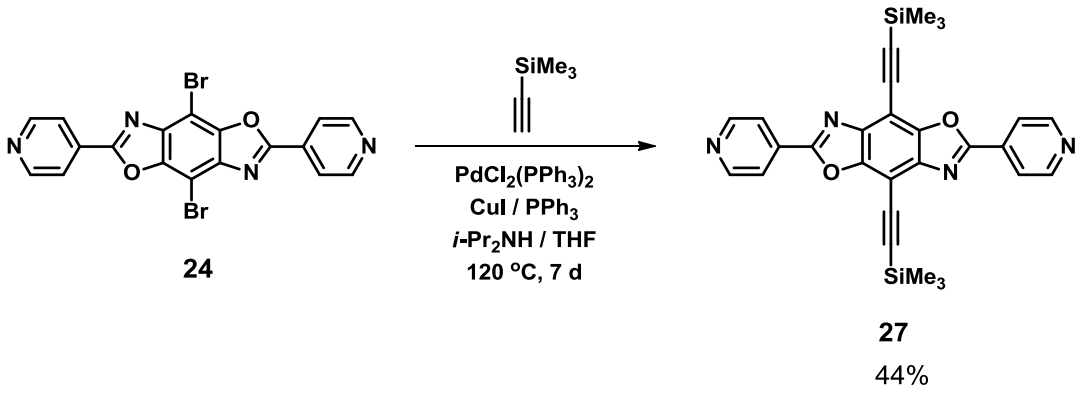

Using a syringe, degassed *i*-Pr_2NH (25 mL) and THF (25 mL) were added to a thick-walled pressure vessel containing 2,6-dipyridin-4-yl-4,8-dibromobenzo[1,2-*d*;4,5-*d*′]bisoxazole (1.60 g, 3.39 mmol), $PdCl_2(PPh_3)_2$ (95.2 mg, 0.136 mmol), CuI (12.9 mg, 0.068 mmol), and PPh_3 (35.6 mg, 0.136 mmol) under the flow of nitrogen gas. The resulting suspension was sonicated for 1 min, and then trimethylsilylacetylene (4.88 mL, 33.9 mmol) was added under nitrogen atmosphere. The vessel was sealed firmly, and the mixture was stirred and heated for 7 d at 120 ^oC. After cooling, the resultant mixture was concentrated under reduced pressure, and the residue was purified by silica gel column chromatography, eluting first with hexane/CH_2Cl_2 mixtures in 90:10 and 75:25 ratios, before switching to pure CH_2Cl_2. The solvent was removed under reduced pressure to yield a light tan powder of compound **27** in 44% yield (752 mg, 1.48 mmol) with mp 323 ℃. UV-Vis (THF): λ_{max} (log ε) = 375 (4.81), 357 (4.92), 342 (4.75), 288 (4.75), 278 (4.66) nm. IR (neat): 2960 (w, $\tilde{\nu}_{C–H}$), 2153 (w, $\tilde{\nu}_{C\equiv C}$), 1608 (w), 1575 (w), 1543 (w), 1488 (w), 1416 (w), 1377 (w), 1336 (w), 1316 (w), 1269 (w), 1250 (w), 1215 (w), 1088 (w), 1079 (w), 1010 (w), 990 (m), 983 (m), 923 (w), 850 (s), 832 (m), 759 (w), 739 (w), 725

(w), 698 (m), 688 (m) cm^{-1}. ^1H NMR ($CDCl_3$, 500 MHz): δ 8.87 (br s, 4H), 8.20 (d, $^3J_{H–H}$ = 5.95 Hz, 4H), 0.42 (s, 18H) ppm. ^{13}C NMR ($CDCl_3$, 125 MHz): δ 162.6, 150.9, 149.5, 141.5, 133.5, 121.4, 108.7, 99.8, 93.4, 0.0 ppm. LRMS (ESI/$[M + H]^+$) calcd for $C_{28}H_{26}N_4O_2Si_2$: 507.16, found 507.45. Anal. Calcd for $C_{34}H_{38}N_4O_2Si_2$: C, 66.37; H, 5.17; N, 11.06. Found: C, 66.06; H, 5.19; N, 10.79.

3.4.4 Synthesis of Cruciform 28

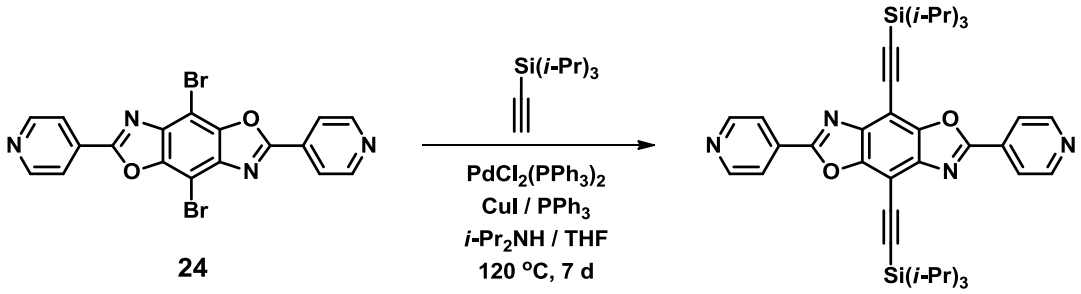

Using a syringe, degassed *i*-Pr_2NH (5 mL) and THF (5 mL) were added to a thick-walled pressure vessel containing 2,6-dipyridin-4-yl-4,8-dibromobenzo[1,2-*d*;4,5-*d'*]bisoxazole (238 mg, 0.50 mmol), $PdCl_2(PPh_3)_2$ (14.2 mg, 0.020 mmol), CuI (1.90 mg, 0.010 mmol), and PPh_3 (5.30 mg, 0.020 mmol) under the flow of nitrogen gas. The resulting suspension was sonicated for 1 min, and then triisopropylsilylacetylene (1.15 mL, 5.04 mmol) was added under nitrogen atmosphere. The vessel was sealed firmly, and the mixture was stirred and heated for 7 d at 120 ^oC. After cooling, the resultant mixture was concentrated under reduced pressure, and the residue was purified by silica gel column chromatography, eluting with hexane/ethyl acetate mixtures (90:10, 80:20, and

67:33 ratios). The solvent was removed under reduced pressure to yield a light brown powder of compound **28** in 54% yield (140 mg, 0.27 mmol) with mp 331 ℃. UV-Vis (THF): λ_{max} (log ε) = 376 (4.68), 359 (4.83), 343 (4.67), 290 (4.65), 280 (4.55) nm. IR (neat): 2942 (m), 2895 (w), 2865 (m), 2157 (w, $\tilde{\nu}_{C\equiv C}$), 1608 (w), 1576 (m), 1545 (w), 1527 (w), 1489 (w), 1464 (w), 1418 (w), 1383 (m), 1270 (m), 1090 (w), 1080 (w), 1064 (m), 1013 (m), 990 (s), 922 (m), 882 (m), 831 (m), 741 (s), 725 (w), 689 (s), 671 (s), 662 (s) cm^{-1}. ^{1}H NMR ($CDCl_3$, 500 MHz): δ 8.87 (d, $^{3}J_{H-H}$ = 5.73 Hz, 4H), 8.14 (d, $^{3}J_{H-H}$ = 6.30 Hz, 4H), 1.27 (m, 42H) ppm. ^{13}C NMR ($CDCl_3$, 125 MHz): δ 162.3, 150.9, 149.7, 141.6, 133.8, 121.3, 105.6, 99.9, 95.7, 18.8, 11.4 ppm. LRMS (ESI/$[M + H]^+$) calcd for $C_{40}H_{50}N_4O_2Si_2$: 675.35, found 675.56. Anal. Calcd for $C_{40}H_{50}N_4O_2Si_2$: C, 71.17; H, 7.47; N, 8.30. Found: C, 70.94; H, 7.64; N, 7.98.

3.4.5 UV/Vis Absorption Spectra for the Titrations of Cruciforms with Anions

UV/Vis absorption titrations were performed using Perkin-Elmer LAMBDA 25 UV/Vis Spectrometer. Sensing solutions of cruciforms **25**–**28** were prepared in THF at the dilution of 1×10^{-5} M. For each analyte, three stock solutions of tetrabutylammonium salts were prepared in THF with the concentrations of 1×10^{-2} M, 1×10^{-3} M, and 1×10^{-4} M. For UV/Vis absorption determination, a 3 mL aliquot of the 1×10^{-5} M solution of the cruciform was placed into a quartz cuvette and was titrated using the 1×10^{-2} M stock solution of tetrabutylammonium salt giving the indicated range of analyte equivalents shown in the graph.

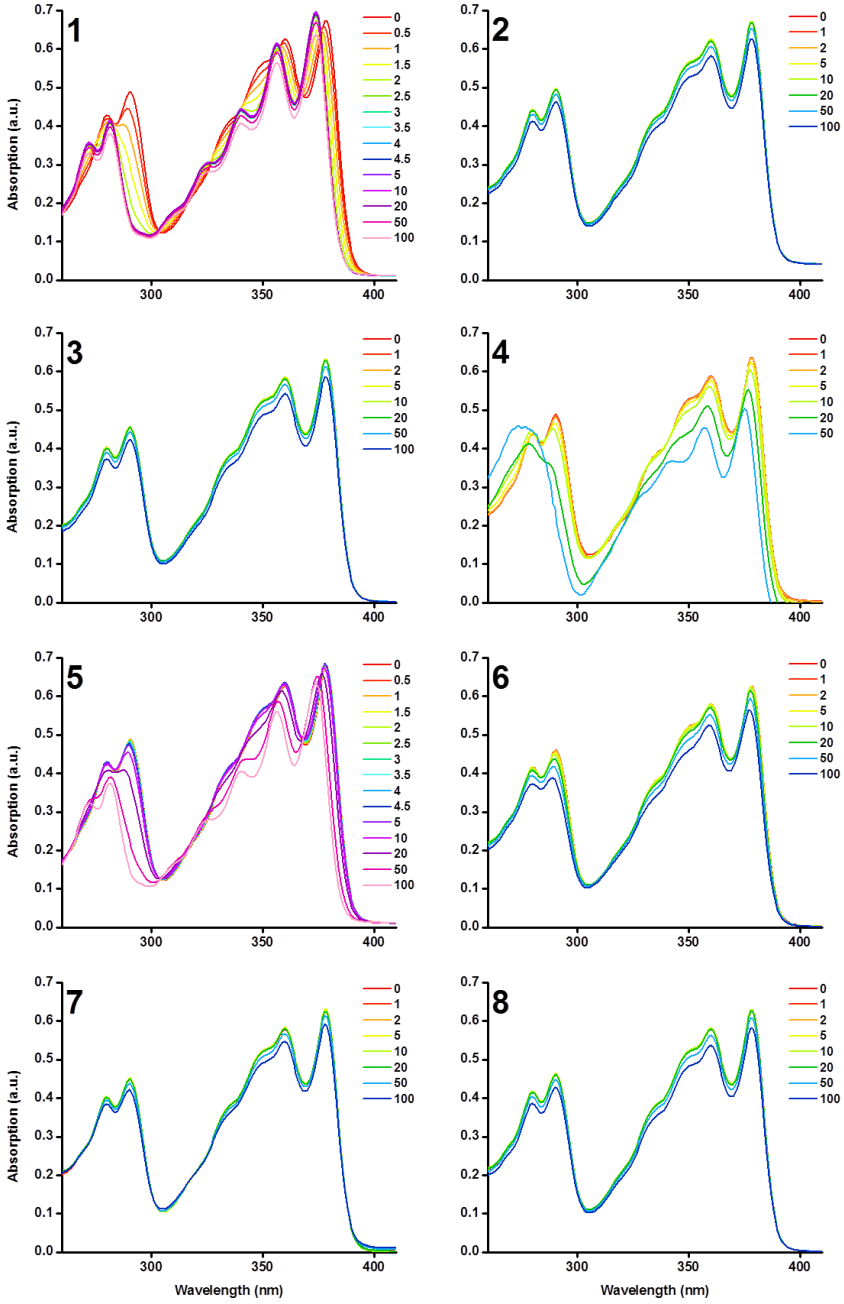

Figure 3.5 UV/Vis absorption spectra for the titration of the 1×10^{-5} M solution of **25** in THF with: (1) fluoride, (2) chloride, (3) bromide, (4) iodide, (5) hydroxide, (6) acetate, (7) phosphate, and (8) nitrate. The numbers on the right side of each graph indicated the number of equivalents of the anion added to the sensing solution. All anions were added as 1×10^{-2} M solutions of the corresponding tetrabutylammonium salts in THF.

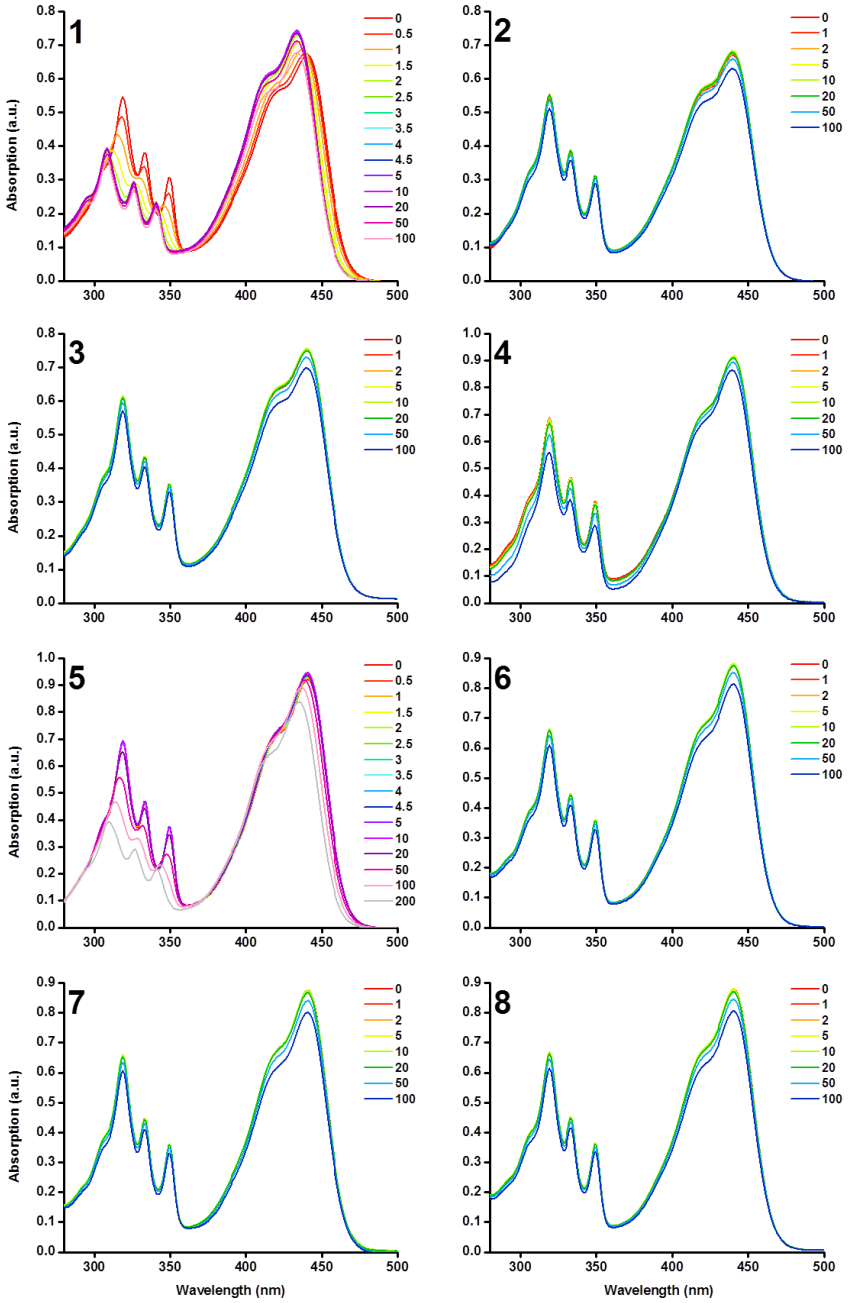

Figure 3.6 UV/Vis absorption spectra for the titration of the 1×10^{-5} M solution of **26** in THF with: (1) fluoride, (2) chloride, (3) bromide, (4) iodide, (5) hydroxide, (6) acetate, (7) phosphate, and (8) nitrate. The numbers on the right side of each graph indicated the number of equivalents of the anion added to the sensing solution. All anions were added as 1×10^{-2} M solutions of the corresponding tetrabutylammonium salts in THF.

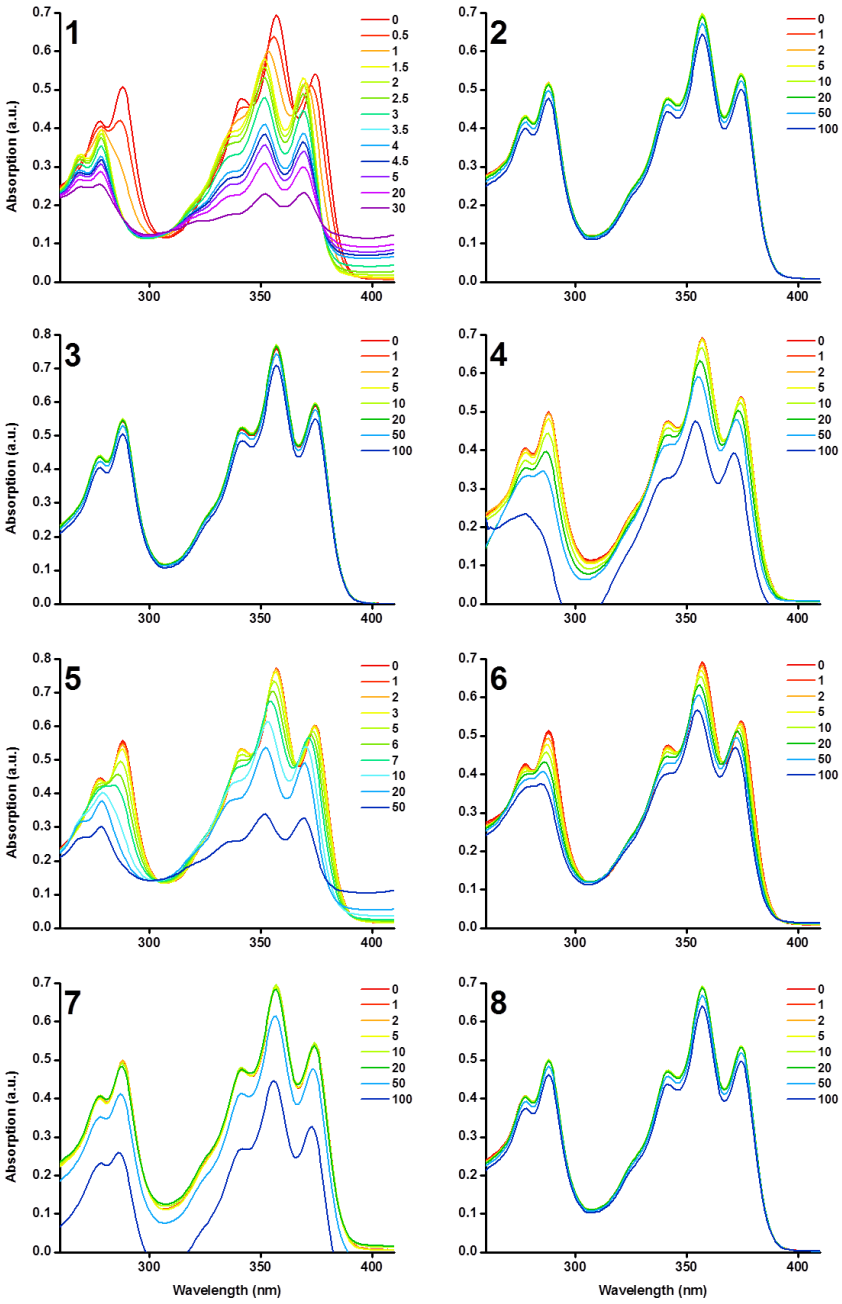

Figure 3.7 UV/Vis absorption spectra for the titration of the 1×10^{-5} M solution of **27** in THF with: (1) fluoride, (2) chloride, (3) bromide, (4) iodide, (5) hydroxide, (6) acetate, (7) phosphate, and (8) nitrate. The numbers on the right side of each graph indicated the number of equivalents of the anion added to the sensing solution. All anions were added as 1×10^{-2} M solutions of the corresponding tetrabutylammonium salts in THF.

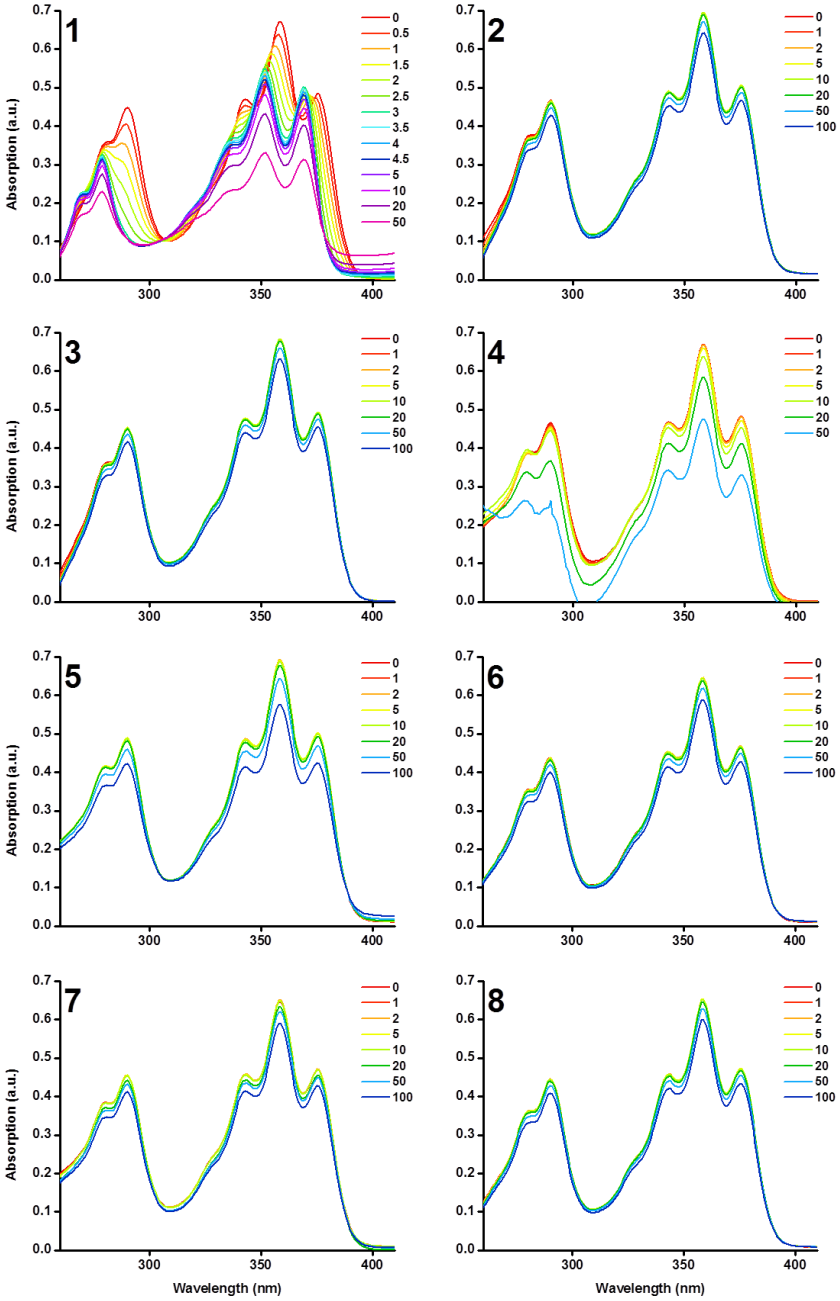

Figure 3.8 UV/Vis absorption spectra for the titration of the 1×10^{-5} M solution of **28** in THF with: (1) fluoride, (2) chloride, (3) bromide, (4) iodide, (5) hydroxide, (6) acetate, (7) phosphate, and (8) nitrate. The numbers on the right side of each graph indicated the number of equivalents of the anion added to the sensing solution. All anions were added as 1×10^{-2} M solutions of the corresponding tetrabutylammonium salts in THF.

3.4.6 Fluorescence Emission Spectra for the Titrations of Cruciforms with Anions

Fluorescence emission titrations were performed using Perkin-Elmer Fluorescence Spectrometer LS-55. Sensing solutions of cruciforms **25**–**28** were prepared in THF at the dilution of 1×10^{-7} M. For each analyte, three stock solutions of tetrabutylammonium salts were prepared in THF with the concentrations of 1×10^{-2} M, 1×10^{-3} M, and 1×10^{-4} M. For fluorescence titrations, a 3 mL aliquot of the 1×10^{-7} M solution of the cruciform was placed into a quartz cuvette and was titrated using first the 1×10^{-4} M, then the 1×10^{-3} M, and finally the 1×10^{-2} M stock solutions of the tetrabutylammonium salt, to give the indicated range of analyte equivalents shown in the graph (1 to 5,000 equivalents). The excitation wavelength used for fluorescence titration corresponds to the isosbestic point which was selected in the UV/Vis spectrum.

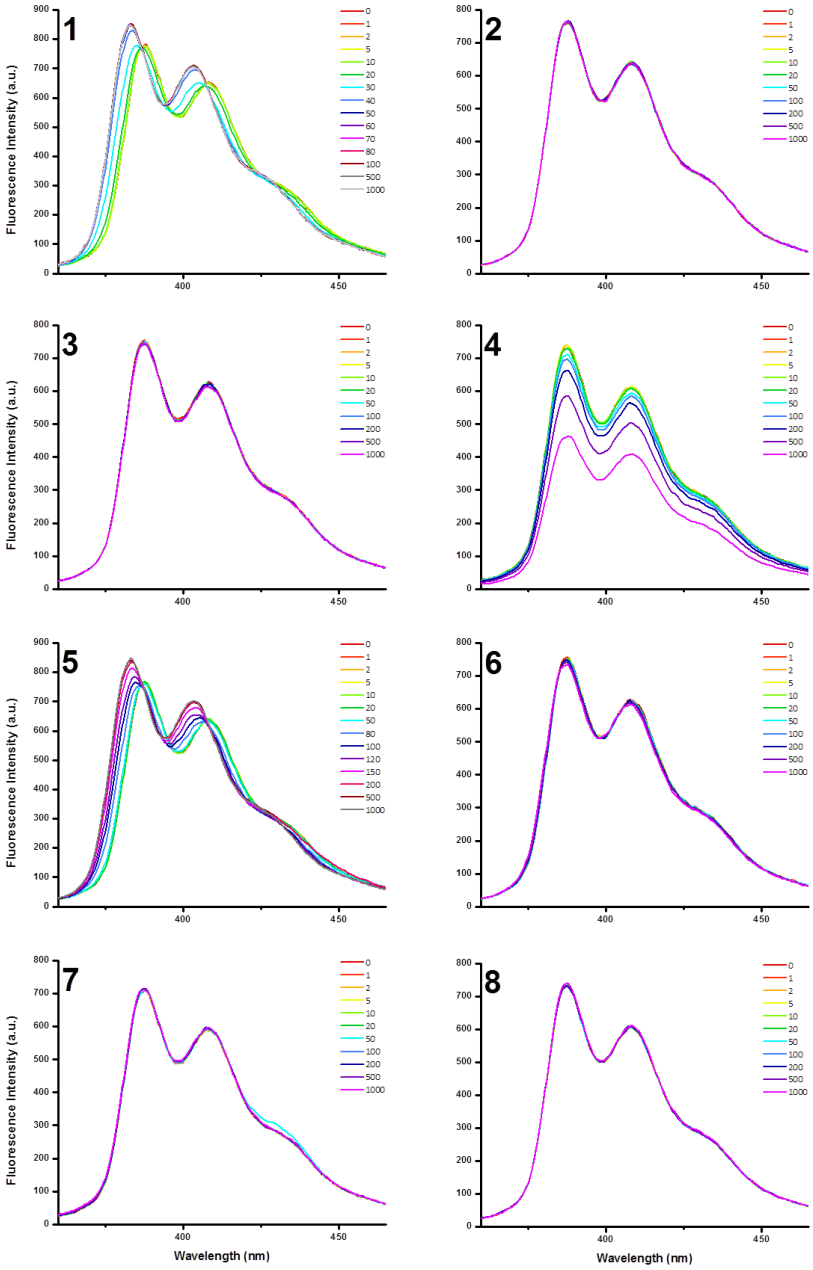

Figure 3.9 Fluorescence emission spectra for the titration of the 1×10^{-7} M solution of **25** in THF with: (1) fluoride, (2) chloride, (3) bromide, (4) iodide, (5) hydroxide, (6) acetate, (7) phosphate, and (8) nitrate. The numbers on the right side of each graph indicated the number of equivalents of the anion added to the sensing solution. Excitation wavelength is 303 nm.

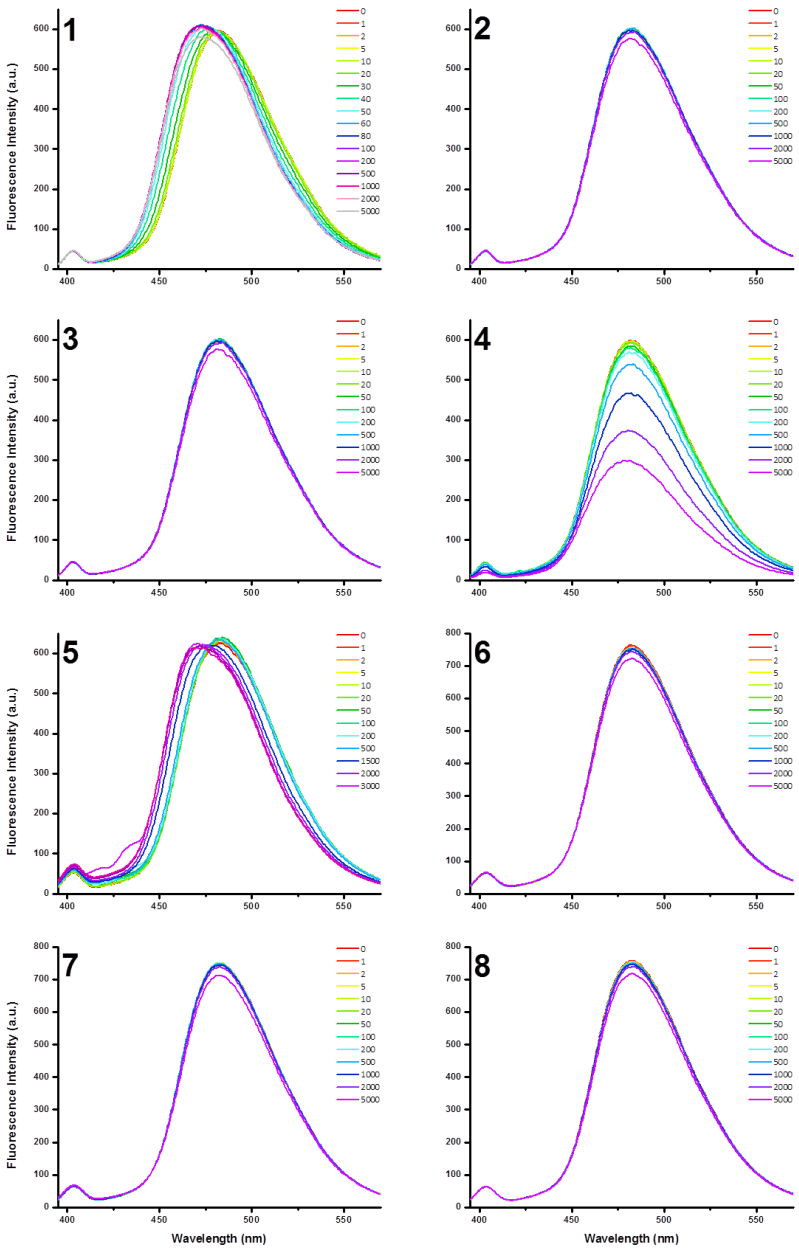

Figure 3.10 Fluorescence emission spectra for the titration of the 1×10^{-7} M solution of **26** in THF with: (1) fluoride, (2) chloride, (3) bromide, (4) iodide, (5) hydroxide, (6) acetate, (7) phosphate, and (8) nitrate. The numbers on the right side of each graph indicated the number of equivalents of the anion added to the sensing solution. Excitation wavelength is 360 nm.

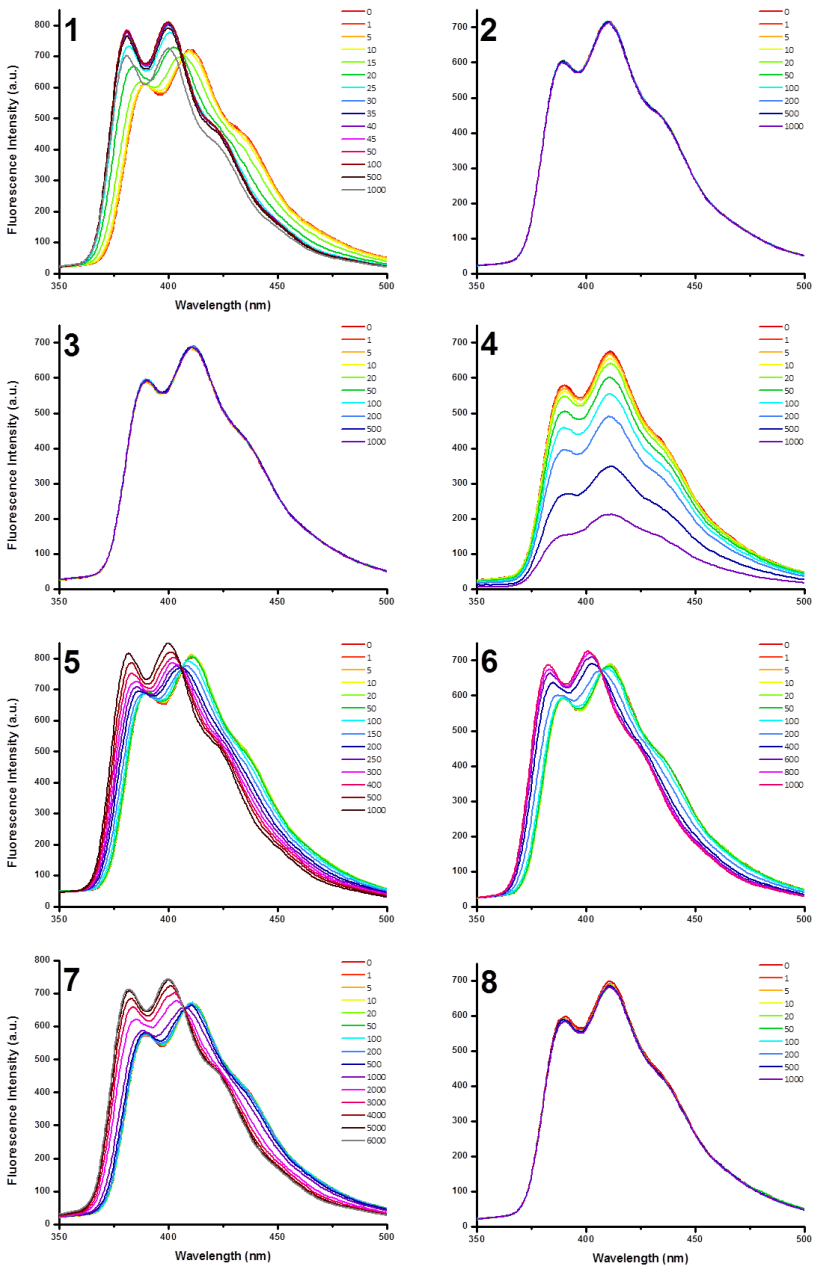

Figure 3.11 Fluorescence emission spectra for the titration of the 1×10^{-7} M solution of **27** in THF with: (1) fluoride, (2) chloride, (3) bromide, (4) iodide, (5) hydroxide, (6) acetate, (7) phosphate, and (8) nitrate. The numbers on the right side of each graph indicated the number of equivalents of the anion added to the sensing solution. Excitation wavelength is 306 nm.

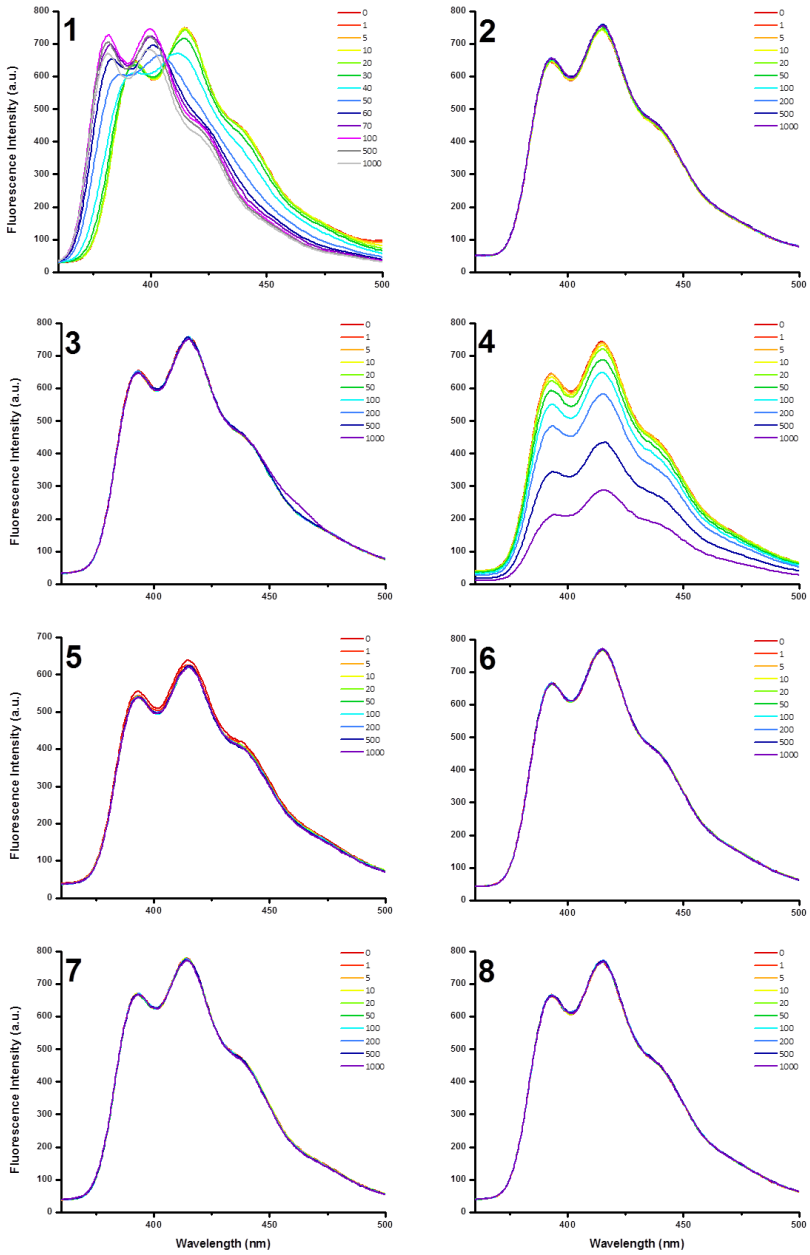

Figure 3.12 Fluorescence emission spectra for the titration of the 1×10^{-7} M solution of **28** in THF with: (1) fluoride, (2) chloride, (3) bromide, (4) iodide, (5) hydroxide, (6) acetate, (7) phosphate, and (8) nitrate. The numbers on the right side of each graph indicated the number of equivalents of the anion added to the sensing solution. Excitation wavelength is 306 nm.

3.4.7 Photography Details

All digital images of emission colors (Figure 3.4) were obtained with a Canon EOS Rebel T3i digital camera, setting a shutter speed from 0.2 s to 0.6 s depending on the fluorophores. To take photographs, vials including sensing solutions and analytes were placed in the hand-made dark box under the UV light provided by UVLS-28 EL series UV lamp (λ_{exc} = 365 nm). Approximately 1 mL of 1×10^{-5} M solution of the corresponding fluorophore was placed into each vial, and anionic analytes were added in tenfold excess. Photographs were immediately taken.

References

1. Gleiter, R.; Haberhauer, G., *Aromaticity and Other Conjugation Effects*. Wiley-VCH: Weinheim, 2012.

2. (a) Chen, K. Y.; Hsieh, H. H.; Wu, C. C.; Hwang, J. J.; Chow, T. J. *Chem. Commun.* **2007**, 1065–1067. (b) Kanibolotsky, A. L.; Perepichka, I. F.; Skabara, P. J. *Chem. Soc. Rev.* **2010**, *39*, 2695–2728. (c) Roncali, J. *Acc. Chem. Res.* **2000**, *33*, 147–156.

3. (a) Wu, J.; Pisula, W.; Mullen, K. *Chem. Rev.* **2007**, *107*, 718–747. (b) Pron, A.; Gawrys, P.; Zagorska, M.; Djurado, D.; Demadrille, R. *Chem. Soc. Rev.* **2010**, *39*, 2577–2632.

4. (a) Delaire, J. A.; Nakatani, K. *Chem. Rev.* **2000**, *100*, 1817–1845. (b) Dsouza, R. N.; Pischel, U.; Nau, W. M. *Chem. Rev.* **2011**, *111*, 7941–7980. (c) Fabian, J.; Nakazumi, H.; Matsuoka, M. *Chem. Rev.* **1992**, *92*, 1197–1226. (d) Hagfeldt, A.; Boschloo, G.; Sun, L.; Kloo, L.; Pettersson, H. *Chem. Rev.* **2010**, *110*, 6595–6663. (e) Merino, E. *Chem. Soc. Rev.* **2011**, *40*, 3835–3853. (f) Rattee, I. D. *Chem. Soc. Rev.* **1972**, *1*, 145–162. (g) Reichardt, C. *Chem. Rev.* **1994**, *94*, 2319–2358.

5. (a) Tang, C. W.; Vanslyke, S. A. *Appl. Phys. Lett.* **1987**, *51*, 913–915. (b) Friend, R. H.; Gymer, R. W.; Holmes, A. B.; Burroughes, J. H.; Marks, R. N.; Taliani, C.; Bradley, D. D. C.; Dos Santos, D. A.; Bredas, J. L.; Logdlund, M.; Salaneck, W. R. *Nature* **1999**, *397*, 121–128. (c) Veinot, J. G. C.; Marks, T. J. *Acc. Chem. Res.* **2005**, *38*, 632–643.

6. (a) Horowitz, G. *Adv. Mater.* **1998**, *10*, 365–377. (b) Dimitrakopoulos, C. D.; Malenfant, P. R. L. *Adv. Mater.* **2002**, *14*, 99–117. (c) Newman, C. R.; Frisbie, C. D.; da Silva, D. A.; Bredas, J. L.; Ewbank, P. C.; Mann, K. R. *Chem. Mater.* **2004**, *16*, 4436–

4451. (d) Murphy, A. R.; Frechet, J. M. J. *Chem. Rev.* **2007**, *107*, 1066–1096. (e) Mas-Torrent, M.; Rovira, C. *Chem. Soc. Rev.* **2008**, *37*, 827–838.

7. (a) Cheng, Y. J.; Yang, S. H.; Hsu, C. S. *Chem. Rev.* **2009**, *109*, 5868–5923. (b) Clifford, J. N.; Martinez-Ferrero, E.; Viterisi, A.; Palomares, E. *Chem. Soc. Rev.* **2011**, *40*, 1635–1646. (c) Haid, S.; Marszalek, M.; Mishra, A.; Wielopolski, M.; Teuscher, J.; Moser, J. E.; Humphry-Baker, R.; Zakeeruddin, S. M.; Gratzel, M.; Bauerle, P. *Adv. Funct. Mater.* **2012**, *22*, 1291–1302.

8. (a) Boens, N.; Leen, V.; Dehaen, W. *Chem. Soc. Rev.* **2012**, *41*, 1130–1172. (b) Chen, X. Q.; Tian, X. Z.; Shin, I.; Yoon, J. *Chem. Soc. Rev.* **2011**, *40*, 4783–4804. (c) Du, J. J.; Hu, M. M.; Fan, J. L.; Peng, X. J. *Chem. Soc. Rev.* **2012**, *41*, 4511–4535. (d) Moragues, M. E.; Martinez-Manez, R.; Sancenon, F. *Chem. Soc. Rev.* **2011**, *40*, 2593–2643. (e) Zhou, Y.; Xu, Z.; Yoon, J. *Chem. Soc. Rev.* **2011**, *40*, 2222–2235. (f) Zhou, Y.; Yoon, J. *Chem. Soc. Rev.* **2012**, *41*, 52–67.

9. (a) Zucchero, A. J.; Wilson, J. N.; Bunz, U. H. F. *J. Am. Chem. Soc.* **2006**, *128*, 11872–11881. (b) Miller, J. J.; Marsden, J. A.; Haley, M. M. *Synlett* **2004**, 165–168. (c) Lim, J.; Albright, T. A.; Martin, B. R.; Miljanić, O. Š. *J. Org. Chem.* **2011**, *76*, 10207–10219. (d) Jung, K. H.; Bae, S. Y.; Kim, K. H.; Cho, M. J.; Lee, K.; Kim, Z. H.; Choi, D. H.; Lee, D. H.; Chung, D. S.; Park, C. E. *Chem. Commun.* **2009**, 5290–5292.

10. (a) Saragi, T. P. I.; Spehr, T.; Siebert, A.; Fuhrmann-Lieker, T.; Salbeck, J. *Chem. Rev.* **2007**, *107*, 1011–1065. (b) Shirota, Y.; Kageyama, H. *Chem. Rev.* **2007**, *107*, 953–1010.

11. (a) Bartholomew, G. P.; Bazan, G. C. *Acc. Chem. Res.* **2001**, *34*, 30–39. (b) Bartholomew, G. P.; Rumi, M.; Pond, S. J. K.; Perry, J. W.; Tretiak, S.; Bazan, G. C. *J. Am. Chem. Soc.* **2004**, *126*, 11529–11542.

12. (a) Bilge, A.; Zen, A.; Forster, M.; Li, H. B.; Galbrecht, F.; Nehls, B. S.; Farrell, T.; Neher, D.; Scherf, U. *J. Mater. Chem.* **2006**, *16*, 3177–3182. (b) Zen, A.; Pingel, P.; Jaiser, F.; Neher, D.; Grenzer, J.; Zhuang, W.; Rabe, J. P.; Bilge, A.; Galbrecht, F.; Nehls, B. S.; Farrell, T.; Scherf, U.; Abellon, R. D.; Grozema, F. C.; Siebbeles, L. D. A. *Chem. Mater.* **2007**, *19*, 1267–1276.

13. (a) Kivala, M.; Diederich, F. *Acc. Chem. Res.* **2009**, *42*, 235–248. (b) Nielsen, M. B.; Diederich, F. *Chem. Rev.* **2005**, *105*, 1837–1867. (c) Anthony, J.; Boldi, A. M.; Rubin, Y.; Hobi, M.; Gramlich, V.; Knobler, C. B.; Seiler, P.; Diederich, F. *Helv. Chim. Acta* **1995**, *78*, 13–45.

14. Tolosa, J.; Diez-Barra, E.; Sanchez-Verdu, P.; Rodriguez-Lopez, J. *Tetrahedron Lett.* **2006**, *47*, 4647–4651.

15. (a) Chase, D. T.; Young, B. S.; Haley, M. M. *J. Org. Chem.* **2011**, *76*, 4043–4051. (b) Marsden, J. A.; Miller, J. J.; Shirtcliff, L. D.; Haley, M. M. *J. Am. Chem. Soc.* **2005**, *127*, 2464–2476. (c) Ohta, K.; Yamada, S.; Kamada, K.; Slepkov, A. D.; Hegmann, F. A.; Tykwinski, R. R.; Shirtcliff, L. D.; Haley, M. M.; Salek, P.; Gel'mukhanov, F.; Agren, H. *J. Phys. Chem. A* **2011**, *115*, 105–117. (d) Samori, S.; Tojo, S.; Fujitsuka, M.; Spitler, E. L.; Haley, M. M.; Majima, T. *J. Org. Chem.* **2007**, *72*, 2785–2793. (e) Samori, S.; Tojo, S.; Fujitsuka, M.; Spitler, E. L.; Haley, M. M.; Majima, T. *J. Org. Chem.* **2008**, *73*, 3551–3558. (f) Slepkov, A. D.; Hegmann, F. A.; Tykwinski, R. R.; Kamada, K.; Ohta, K.; Marsden, J. A.; Spitler, E. L.; Miller, J. J.; Haley, M. M. *Opt. Lett.* **2006**, *31*, 3315–3317.

(g) Spitler, E. L.; Haley, M. M. *Tetrahedron* **2008**, *64*, 11469–11474. (h) Spitler, E. L.; Monson, J. M.; Haley, M. M. *J. Org. Chem.* **2008**, *73*, 2211–2223. (i) Spitler, E. L.; Shirtcliff, L. D.; Haley, M. M. *J. Org. Chem.* **2007**, *72*, 86–96.

16. (a) Brombosz, S. M.; Zucchero, A. J.; Phillips, R. L.; Vazquez, D.; Wilson, A.; Bunz, U. H. F. *Org. Lett.* **2007**, *9*, 4519–4522. (b) Davey, E. A.; Zucchero, A.; Trapp, O.; Bunz, U. H. F. *J. Am. Chem. Soc.* **2011**, *133*, 7716–7718. (c) Gard, M. N.; Zucchero, A. J.; Kuzmanich, G.; Oelsner, C.; Guldi, D.; Dreuw, A.; Bunz, U. H. F.; Garcia-Garibay, M. A. *Org. Lett.* **2012**, *14*, 1000–1003. (d) Gerhardt, W. W.; Zucchero, A. J.; South, C. R.; Bunz, U. H. F.; Weck, M. *Chem. Eur. J.* **2007**, *13*, 4467–4474. (e) Gerhardt, W. W.; Zucchero, A. J.; Wilson, J. N.; South, C. R.; Bunz, U. H. F.; Weck, M. *Chem. Commun.* **2006**, 2141–2143. (f) Hauck, M.; Schonhaber, J.; Zucchero, A. J.; Hardcastle, K. I.; Muller, T. J. J.; Bunz, U. H. F. *J. Org. Chem.* **2007**, *72*, 6714–6725. (g) McGrier, P. L.; Solntsev, K. M.; Miao, S.; Tolbert, L. M.; Miranda, O. R.; Rotello, V. M.; Bunz, U. H. F. *Chem. Eur. J.* **2008**, *14*, 4503–4510. (h) McGrier, P. L.; Solntsev, K. M.; Schonhaber, J.; Brombosz, S. M.; Tolbert, L. M.; Bunz, U. H. F. *Chem. Commun.* **2007**, 2127–2129. (i) McGrier, P. L.; Solntsev, K. M.; Zucchero, A. J.; Miranda, O. R.; Rotello, V. M.; Tolbert, L. M.; Bunz, U. H. F. *Chem. Eur. J.* **2011**, *17*, 3112–3119. (j) Patze, C.; Broedner, K.; Rominger, F.; Trapp, O.; Bunz, U. H. F. *Chem. Eur. J.* **2011**, *17*, 13720–13725. (k) Schwaebel, T.; Schaefer, V.; Wenz, J.; Coombs, B. A.; Tolosa, J.; Bunz, U. H. F. *J. Org. Chem.* **2013**, *78*, 960–965. (l) Tolosa, J.; Bunz, U. H. F. *Chem. Asian J.* **2009**, *4*, 270–276. (m) Tolosa, J.; Solntsev, K. M.; Tolbert, L. M.; Bunz, U. H. F. *J. Org. Chem.* **2010**, *75*, 523–534. (n) Tolosa, J.; Zucchero, A. J.; Bunz, U. H. F. *J. Am. Chem. Soc.* **2008**, *130*, 6498–6506. (o) Wilson, J. N.; Bunz, U. H. F. *J. Am. Chem. Soc.* **2005**, *127*, 4124–4125.

(p) Wilson, J. N.; Josowicz, M.; Wang, Y. Q.; Bunz, U. H. F. *Chem. Commun.* **2003**, 2962–2963. (q) Wilson, J. N.; Smith, M. D.; Enkelmann, V.; Bunz, U. H. F. *Chem. Commun.* **2004**, 1700–1701. (r) Zucchero, A. J.; Shiels, R. A.; McGrier, P. L.; To, M. A.; Jones, C. W.; Bunz, U. H. F. *Chem. Asian J.* **2009**, *4*, 262–269. (s) Zucchero, A. J.; McGrier, P. L.; Bunz, U. H. F. *Acc. Chem. Res.* **2010**, *43*, 397–408.

17. (a) Lim, J.; Miljanić, O. Š. *Chem. Commun.* **2012**, *48*, 10301–10303. (b) Lim, J.; Nam, D.; Miljanić, O. Š. *Chem. Sci.* **2012**, *3*, 559–563. (c) Lim, J.; Osowska, K.; Armitage, J. A.; Martin, B. R.; Miljanić, O. Š. *CrystEngComm* **2012**, *14*, 6152–6162. (d) Osowska, K.; Miljanić, O. Š. *Chem. Commun.* **2010**, *46*, 4276–4278.

18. (a) Klare, J. E.; Tulevski, G. S.; Sugo, K.; de Picciotto, A.; White, K. A.; Nuckolls, C. *J. Am. Chem. Soc.* **2003**, *125*, 6030–6031. (b) Klare, J. E.; Tulevski, G. S.; Nuckolls, C. *Langmuir* **2004**, *20*, 10068–10072. (c) Florio, G. M.; Klare, J. E.; Pasamba, M. O.; Werblowsky, T. L.; Hyers, M.; Berne, B. J.; Hybertsen, M. S.; Nuckolls, C.; Flynn, G. W. *Langmuir* **2006**, *22*, 10003–10008.

19. (a) Intemann, J. J.; Hellerich, E. S.; Tlach, B. C.; Ewan, M. D.; Barnes, C. A.; Bhuwalka, A.; Cai, M.; Shinar, J.; Shinar, R.; Jeffries-EL, M. *Macromolecules* **2012**, *45*, 6888–6897. (b) Tlach, B. C.; Tomlinson, A. L.; Bhuwalka, A.; Jeffries-EL, M. *J. Org. Chem.* **2011**, *76*, 8670–8681.

20. (a) Batten, S. R.; Champness, N. R.; Chen, X. M.; Garcia-Martinez, J.; Kitagawa, S.; Ohrstrom, L.; O'Keeffe, M.; Suh, M. P.; Reedijk, J. *CrystEngComm* **2012**, *14*, 3001–3004. (b) Chen, B. L.; Xiang, S. C.; Qian, G. D. *Acc. Chem. Res.* **2010**, *43*, 1115–1124. (c) Ferey, G. *Chem. Soc. Rev.* **2008**, *37*, 191–214. (d) Kitagawa, S.; Kitaura, R.; Noro, S. *Angew. Chem. Int. Ed.* **2004**, *43*, 2334–2375. (e) Maspoch, D.; Ruiz-Molina, D.; Veciana,

J. *Chem. Soc. Rev.* **2007**, *36*, 770–818. (f) Rao, C. N. R.; Natarajan, S.; Vaidhyanathan, R. *Angew. Chem. Int. Ed.* **2004**, *43*, 1466–1496. (g) Yaghi, O. M.; O'Keeffe, M.; Ockwig, N. W.; Chae, H. K.; Eddaoudi, M.; Kim, J. *Nature* **2003**, *423*, 705–714.

21. (a) Getman, R. B.; Bae, Y. S.; Wilmer, C. E.; Snurr, R. Q. *Chem. Rev.* **2012**, *112*, 703–723. (b) Suh, M. P.; Park, H. J.; Prasad, T. K.; Lim, D. W. *Chem. Rev.* **2012**, *112*, 782–835. (c) Sumida, K.; Rogow, D. L.; Mason, J. A.; McDonald, T. M.; Bloch, E. D.; Herm, Z. R.; Bae, T. H.; Long, J. R. *Chem. Rev.* **2012**, *112*, 724–781. (d) Wu, H. H.; Gong, Q. H.; Olson, D. H.; Li, J. *Chem. Rev.* **2012**, *112*, 836–868. (e) Collins, D. J.; Zhou, H. C. *J. Mater. Chem.* **2007**, *17*, 3154–3160. (f) Eddaoudi, M.; Kim, J.; Rosi, N.; Vodak, D.; Wachter, J.; O'Keeffe, M.; Yaghi, O. M. *Science* **2002**, *295*, 469–472. (g) Farha, O. K.; Yazaydin, A. O.; Eryazici, I.; Malliakas, C. D.; Hauser, B. G.; Kanatzidis, M. G.; Nguyen, S. T.; Snurr, R. Q.; Hupp, J. T. *Nat. Chem.* **2010**, *2*, 944–948. (h) Li, J. R.; Ma, Y. G.; McCarthy, M. C.; Sculley, J.; Yu, J. M.; Jeong, H. K.; Balbuena, P. B.; Zhou, H. C. *Coord. Chem. Rev.* **2011**, *255*, 1791–1823. (i) Rowsell, J. L. C.; Yaghi, O. M. *J. Am. Chem. Soc.* **2006**, *128*, 1304–1315. (j) Sumida, K.; Brown, C. M.; Herm, Z. R.; Chavan, S.; Bordiga, S.; Long, J. R. *Chem. Commun.* **2011**, *47*, 1157–1159.

22. (a) Li, J. R.; Sculley, J.; Zhou, H. C. *Chem. Rev.* **2012**, *112*, 869–932. (b) Chen, J.; Zhang, J.; Li, J.; Fu, F.; Yang, H.-H.; Chen, G. *Chem. Commun.* **2010**, *46*, 5939–5941. (c) Li, J. R.; Kuppler, R. J.; Zhou, H. C. *Chem. Soc. Rev.* **2009**, *38*, 1477–1504. (d) Li, K. H.; Olson, D. H.; Seidel, J.; Emge, T. J.; Gong, H. W.; Zeng, H. P.; Li, J. *J. Am. Chem. Soc.* **2009**, *131*, 10368–10369.

23. (a) Seo, J. S.; Whang, D.; Lee, H.; Jun, S. I.; Oh, J.; Jeon, Y. J.; Kim, K. *Nature* **2000**, *404*, 982–986. (b) Dybtsev, D. N.; Nuzhdin, A. L.; Chun, H.; Bryliakov, K. P.;

Talsi, E. P.; Fedin, V. P.; Kim, K. *Angew. Chem. Int. Ed.* **2006**, *45*, 916–920. (c) Wu, C. D.; Hu, A.; Zhang, L.; Lin, W. B. *J. Am. Chem. Soc.* **2005**, *127*, 8940–8941. (d) Farrusseng, D.; Aguado, S.; Pinel, C. *Angew. Chem. Int. Ed.* **2009**, *48*, 7502–7513. (e) Hwang, I. H.; Bae, J. M.; Kim, W.-S.; Jo, Y. D.; Kim, C.; Kim, Y.; Kim, S.-J.; Huh, S. *Dalton Trans.* **2012**, *41*, 12759–12765. (f) Lee, J.; Farha, O. K.; Roberts, J.; Scheidt, K. A.; Nguyen, S. T.; Hupp, J. T. *Chem. Soc. Rev.* **2009**, *38*, 1450–1459. (g) Farha, O. K.; Shultz, A. M.; Sarjeant, A. A.; Nguyen, S. T.; Hupp, J. T. *J. Am. Chem. Soc.* **2011**, *133*, 5652–5655.

24. (a) Chandra, D.; Bhaumik, A. *J. Mater. Chem.* **2009**, *19*, 1901–1907. (b) James, S. L. *Chem. Soc. Rev.* **2003**, *32*, 276–288. (c) Lim, M. H.; Blanford, C. F.; Stein, A. *J. Am. Chem. Soc.* **1997**, *119*, 4090–4091.

25. (a) Lin, W.; Xiu, Y.; Jiang, H.; Zhang, R.; Hildreth, O.; Moon, K.-S.; Wong, C. P. *J. Am. Chem. Soc.* **2008**, *130*, 9636–9637. (b) Horcajada, P.; Chalati, T.; Serre, C.; Gillet, B.; Sebrie, C.; Baati, T.; Eubank, J. F.; Heurtaux, D.; Clayette, P.; Kreuz, C.; Chang, J. S.; Hwang, Y. K.; Marsaud, V.; Bories, P. N.; Cynober, L.; Gil, S.; Ferey, G.; Couvreur, P.; Gref, R. *Nat. Mater.* **2010**, *9*, 172–178.

26. (a) Cui, Y.; Yue, Y.; Qian, G.; Chen, B. *Chem. Rev.* **2012**, *112*, 1126–1162. (b) Kreno, L. E.; Leong, K.; Farha, O. K.; Allendorf, M.; Van Duyne, R. P.; Hupp, J. T. *Chem. Rev.* **2012**, *112*, 1105–1125. (c) Reineke, T. M.; Eddaoudi, M.; Fehr, M.; Kelley, D.; Yaghi, O. M. *J. Am. Chem. Soc.* **1999**, *121*, 1651–1657.

27. (a) Imaz, I.; Maspoch, D.; Rodriguez-Blanco, C.; Perez-Falcon, J. M.; Campo, J.; Ruiz-Molina, D. *Angew. Chem. Int. Ed.* **2008**, *47*, 1857–1860. (b) Kahn, O.; Martinez, C.

J. *Science* **1998**, *279*, 44–48. (c) Coronado, E.; Galan-Mascaros, J. R.; Gomez-Garcia, C. J.; Laukhin, V. *Nature* **2000**, *408*, 447–449.

28. (a) McKinlay, A. C.; Morris, R. E.; Horcajada, P.; Ferey, G.; Gref, R.; Couvreur, P.; Serre, C. *Angew. Chem. Int. Ed.* **2010**, *49*, 6260–6266. (b) Rieter, W. J.; Taylor, K. M. L.; An, H.; Lin, W.; Lin, W. *J. Am. Chem. Soc.* **2006**, *128*, 9024–9025.

29. Yaghi, O. M.; Li, G. M.; Li, H. L. *Nature* **1995**, *378*, 703–706.

30. Kondo, M.; Yoshitomi, T.; Seki, K.; Matsuzaka, H.; Kitagawa, S. *Angew. Chem. Int. Ed.* **1997**, *36*, 1725–1727.

31. Yaghi, O. M.; Davis, C. E.; Li, G. M.; Li, H. L. *J. Am. Chem. Soc.* **1997**, *119*, 2861–2868.

32. Li, H.; Eddaoudi, M.; O'Keeffe, M.; Yaghi, O. M. *Nature* **1999**, *402*, 276–279.

33. Czaja, A. U.; Trukhan, N.; Mueller, U. *Chem. Soc. Rev.* **2009**, *38*, 1284–1293.

34. Schüth, F.; Sing, K. S. W.; Weitkamp, J., *Handbook of Porous Solids*. Wiley-VCH: Weinheim ; Cambridge, 2002.

35. Chae, H. K.; Siberio-Perez, D. Y.; Kim, J.; Go, Y.; Eddaoudi, M.; Matzger, A. J.; O'Keeffe, M.; Yaghi, O. M. *Nature* **2004**, *427*, 523–527.

36. Ma, B. Q.; Mulfort, K. L.; Hupp, J. T. *Inorg. Chem.* **2005**, *44*, 4912–4914.

37. (a) Banerjee, R.; Phan, A.; Wang, B.; Knobler, C.; Furukawa, H.; O'Keeffe, M.; Yaghi, O. M. *Science* **2008**, *319*, 939–943. (b) Park, K. S.; Ni, Z.; Cote, A. P.; Choi, J. Y.; Huang, R. D.; Uribe-Romo, F. J.; Chae, H. K.; O'Keeffe, M.; Yaghi, O. M. *Proc. Natl. Acad. Sci. USA* **2006**, *103*, 10186–10191. (c) Tan, J. C.; Bennett, T. D.; Cheetham, A. K. *Proc. Natl. Acad. Sci. USA* **2010**, *107*, 9938–9943. (d) Zhang, J. P.; Zhang, Y. B.; Lin, J.

B.; Chen, X. M. *Chem. Rev.* **2012**, *112*, 1001–1033. (e) Hayashi, H.; Cote, A. P.; Furukawa, H.; O'Keeffe, M.; Yaghi, O. M. *Nat. Mater.* **2007**, *6*, 501–506.

38. (a) Tranchemontagne, D. J.; Mendoza-Cortes, J. L.; O'Keeffe, M.; Yaghi, O. M. *Chem. Soc. Rev.* **2009**, *38*, 1257–1283. (b) Robson, R. *J. Chem. Soc., Dalton Trans.* **2000**, 3735–3744. (c) Moulton, B.; Zaworotko, M. J. *Chem. Rev.* **2001**, *101*, 1629–1658. (d) Kim, J.; Chen, B. L.; Reineke, T. M.; Li, H. L.; Eddaoudi, M.; Moler, D. B.; O'Keeffe, M.; Yaghi, O. M. *J. Am. Chem. Soc.* **2001**, *123*, 8239–8247.

39. Seo, Y. K.; Hundal, G.; Jang, I. T.; Hwang, Y. K.; Jun, C. H.; Chang, J. S. *Micropor. Mesopor. Mat.* **2009**, *119*, 331–337.

40. (a) Falcaro, P.; Buso, D.; Hill, A. J.; Doherty, C. M. *Adv. Mater.* **2012**, *24*, 3153–3168. (b) Witters, D.; Vergauwe, N.; Ameloot, R.; Vermeir, S.; De Vos, D.; Puers, R.; Sels, B.; Lammertyn, J. *Adv. Mater.* **2012**, *24*, 1316–1320.

41. Garcia Marquez, A.; Horcajada, P.; Grosso, D.; Ferey, G.; Serre, C.; Sanchez, C.; Boissiere, C. *Chem. Commun.* **2013**, *49*, 3848–3850.

42. (a) Klimakow, M.; Klobes, P.; Rademann, K.; Emmerling, F. *Micropor. Mesopor. Mat.* **2012**, *154*, 113–118. (b) Klimakow, M.; Klobes, P.; Thunemann, A. F.; Rademann, K.; Emmerling, F. *Chem. Mater.* **2010**, *22*, 5216–5221. (c) Yuan, W. B.; Garay, A. L.; Pichon, A.; Clowes, R.; Wood, C. D.; Cooper, A. I.; James, S. L. *CrystEngComm* **2010**, *12*, 4063–4065.

43. Thompson, J. A.; Chapman, K. W.; Koros, W. J.; Jones, C. W.; Nair, S. *Micropor. Mesopor. Mat.* **2012**, *158*, 292–299.

44. Li, M. Y.; Dincă, M. *J. Am. Chem. Soc.* **2011**, *133*, 12926–12929.

45. Wang, Z. Q.; Cohen, S. M. *Chem. Soc. Rev.* **2009**, *38*, 1315–1329.

46. Dincă, M.; Long, J. R. *Angew. Chem. Int. Ed.* **2008**, *47*, 6766–6779.

47. Das, S.; Kim, H.; Kim, K. *J. Am. Chem. Soc.* **2009**, *131*, 3814–3815.

48. Wong-Foy, A. G.; Matzger, A. J.; Yaghi, O. M. *J. Am. Chem. Soc.* **2006**, *128*, 3494–3495.

49. Ferey, G.; Mellot-Draznieks, C.; Serre, C.; Millange, F.; Dutour, J.; Surble, S.; Margiolaki, I. *Science* **2005**, *309*, 2040–2042.

50. (a) Cavka, J. H.; Jakobsen, S.; Olsbye, U.; Guillou, N.; Lamberti, C.; Bordiga, S.; Lillerud, K. P. *J. Am. Chem. Soc.* **2008**, *130*, 13850–13851. (b) Farha, O. K.; Spokoyny, A. M.; Mulfort, K. L.; Hawthorne, M. F.; Mirkin, C. A.; Hupp, J. T. *J. Am. Chem. Soc.* **2007**, *129*, 12680–12681.

51. Chun, H.; Dybtsev, D. N.; Kim, H.; Kim, K. *Chem. Eur. J.* **2005**, *11*, 3521–3529.

52. Morris, W.; Volosskiy, B.; Demir, S.; Gandara, F.; McGrier, P. L.; Furukawa, H.; Cascio, D.; Stoddart, J. F.; Yaghi, O. M. *Inorg. Chem.* **2012**, *51*, 6443–6445.

53. (a) Holmes, B. T.; Pennington, W. T.; Hanks, T. W. *Synth. Commun.* **2003**, *33*, 2447–2461. (b) Ziessel, R.; Suffert, J.; Youinou, M. T. *J. Org. Chem.* **1996**, *61*, 6535–6546.

54. Chen, B. L.; Liang, C. D.; Yang, J.; Contreras, D. S.; Clancy, Y. L.; Lobkovsky, E. B.; Yaghi, O. M.; Dai, S. *Angew. Chem. Int. Ed.* **2006**, *45*, 1390–1393.

55. Koeberl, M.; Cokoja, M.; Bechlars, B.; Herdtweck, E.; Kuehn, F. E. *Dalton Trans.* **2011**, *40*, 11490–11496.

56. (a) Li, Y.-W.; Zhao, J.-P.; Wang, L.-F.; Bu, X.-H. *CrystEngComm* **2011**, *13*, 6002–6006. (b) Zhang, T.-Z.; Lu, Y.; Li, Y.-G.; Zhang, Z.; Chen, W.-L.; Fu, H.; Wang, E.-B. *Inorg. Chim. Acta* **2012**, *384*, 219–224.

57. Murray, L. J.; Dinca, M.; Yano, J.; Chavan, S.; Bordiga, S.; Brown, C. M.; Long, J. R. *J. Am. Chem. Soc.* **2010**, *132*, 7856–7857.

58. (a) Farha, O. K.; Hupp, J. T. *Acc. Chem. Res.* **2010**, *43*, 1166–1175. (b) Farha, O. K.; Mulfort, K. L.; Thorsness, A. M.; Hupp, J. T. *J. Am. Chem. Soc.* **2008**, *130*, 8598–8599. (c) Keene, T. D.; Price, D. J.; Kepert, C. J. *Dalton Trans.* **2011**, *40*, 7122–7126.

59. Wang, Z. Q.; Cohen, S. M. *J. Am. Chem. Soc.* **2007**, *129*, 12368–12369.

60. Zhu, W. T.; He, C.; Wu, P. Y.; Wu, X.; Duan, C. Y. *Dalton Trans.* **2012**, *41*, 3072–3077.

61. Heck, R. F., *Palladium Reagents in Organic Synthesis*. Academic Press: London ; Orlando Fla., 1985; p xx, 461 p.

62. Ling, A. R. *J. Chem. Soc., Trans.* **1892**, *61*, 558–581.

63. Hegedus, L. S.; Odle, R. R.; Winton, P. M.; Weider, P. R. *J. Org. Chem.* **1982**, *47*, 2607–2613.

64. Feldman, A. K.; Steigerwald, M. L.; Guo, X. F.; Nuckolls, C. *Acc. Chem. Res.* **2008**, *41*, 1731–1741.

65. Lirag, R. C.; Le, H. T. M.; Miljanić, O. Š. *Chem. Commun.* **2013**, *49*, 4304–4306.

66. Kumpf, J.; Bunz, U. H. F. *Chem. Eur. J.* **2012**, *18*, 8921–8924.

67. Sanderson, R. T., *Chemical Bonds and Bond Energy*. 2d ed.; Academic Press: New York, 1976.

68. (a) Jung, M. E.; Xia, H. *Tetrahedron Lett.* **1988**, *29*, 297–300. (b) Kim, Y.; Kim, M.; Gabbaï, F. P. *Org. Lett.* **2010**, *12*, 600–602. (c) Lenormand, H.; Goddard, J. P.; Fensterbank, L. *Org. Lett.* **2013**, *15*, 748–751. (d) Tamao, K.; Hayashi, T.; Ito, Y. *J.*

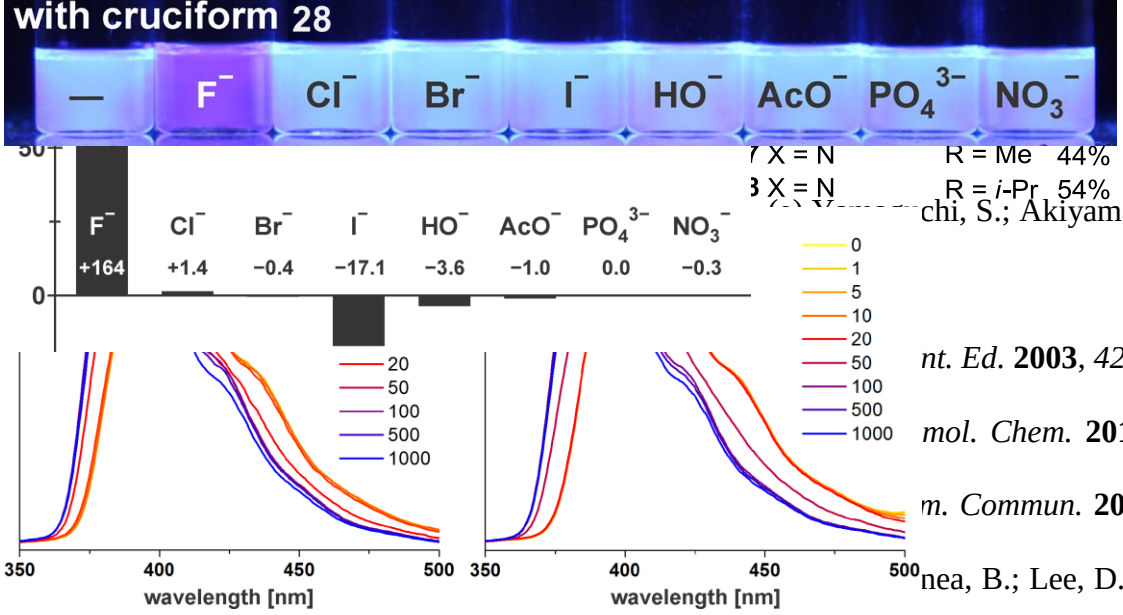

chi, S.; Akiyama, S.; Tamao, K. *J. Am. nt. Ed.* **2003**, *42*, 4803–4806. *mol. Chem.* **2012**, *10*, 3595–3599. (b) *m. Commun.* **2011**, *47*, 3957–3959. (c) nea, B.; Lee, D. W. *Org. Lett.* **2007**, *9*, 3579–3582. (d) Ke, B. W.; Chen, W. X.; Ni, N. T.; Cheng, Y. F.; Dai, C. F.; Dinh, H.; Wang, B. H. *Chem. Commun.* **2013**, *49*, 2494–2496. (e) Kim, D.; Singha, S.; Wang, T.; Seo, E.; Lee, J. H.; Lee, S.-J.; Kim, K. H.; Ahn, K. H. *Chem. Commun.* **2012**, *48*, 10243–10245. (f) Kim, S. Y.; Park, J.; Koh, M.; Park, S. B.; Hong, J. I. *Chem. Commun.* **2009**, 4735–4737. (g) Zheng, F. Y.; Zeng, F.; Yu, C. M.; Hou, X. F.; Wu, S. Z. *Chem. Eur. J.* **2013**, *19*, 936–942.

71. Wuts, P. G. M.; Greene, T. W., *Greene's Protective Groups in Organic Synthesis*. 4th ed.; Wiley-Interscience: Hoboken, N.J., 2007; p xxviii, 1082 p.

72. Albright, T. A.; Burdett, J. K.; Whangbo, M.-H., *Orbital Interactions in Chemistry*. 2nd ed. ed.; Wiley: Hoboken, NJ, 2013.